Agrivoltaics can reduce heat exposure for farmworkers

Talitha H. Neesham-McTiernan[1], Patrick Murphy[1], Greg A. Barron-Gafford[1]

[1]The University of Arizona, 1200 E University Blvd, Tucson, AZ, 85721, USA.

Preprint

This manuscript has not been peer reviewed. It is posted on EarthArXiv to facilitate early sharing of research findings. Feedback is welcome.

Abstract

Heat exposure endangers over 850 million farmworkers, with agricultural labor projected to account for 60% of heat-related working-hour losses by 2030. Agrivoltaic systems, which integrate solar panels with agriculture, may reduce this risk by modifying the thermal environment farmworkers operate within, yet their impact on heat exposure remains unquantified. We evaluate wet bulb globe temperature (WBGT) across conventional full-sun agriculture and four agrivoltaic designs differing in panel height, density, and layout. Agrivoltaic systems significantly reduced WBGT, but the magnitude and timing of cooling varied by design. Overhead systems provided shading throughout the day, and consistently reduced daytime WBGT, with greater panel coverage increasing protection. Conversely, interspaced systems reduced morning and evening exposure but intensified midday heat, as restricted airflow and direct solar radiation elevated WBGT, particularly with lower solar panels. These findings demonstrate that strategic agrivoltaic design can improve farmworker thermal safety, whereas poorly configured systems may exacerbate exposure.

Introduction

Occupational heat exposure threatens the health and safety of the 850 million farmworkers who sustain the global food system (El Khayat et al., 2022; Kjellstrom et al., 2019; Petropoulos et al., 2021; Tigchelaar et al., 2020). Subjected to high temperatures and direct sunlight, farmworkers endure physically demanding labor, often with limited access to cooling resources or adequate shaded rest breaks (Cheney et al., 2022; Edgerly et al., 2024; El Khayat et al., 2022; Moyce et al., 2017; NIOSH, 2016). Under these conditions, the body's cooling mechanisms can quickly become overwhelmed (Budd, 2008; Hanna & Tait, 2015; Havenith & Fiala, 2015; Sawka et al., 2011), with consequences ranging from reduced productivity and cognitive impairment, to heat stroke, and death (Flouris et al., 2018; Helou et al., 2012; Morabito et al., 2020; Moyce et al., 2017; Piil et al., 2020).

Climate change is intensifying these already dangerous conditions (Lüthi et al., 2023; Mitchell et al., 2016; Mora et al., 2017; Raymond et al., 2020; Tigchelaar et al., 2020). Rising temperatures are projected to reduce agricultural labor capacity, with the sector expected to account for 60% of all working hours lost due to heat stress by 2030 (Kjellstrom et al., 2019). These temperature increases will expose growing numbers of farmworkers to heat conditions beyond their body's cooling capacity (Powis et al., 2023), with 2.8% of global farmworkers facing unsurvivable heat conditions under the projected 2 °C of

Corresponding author: Talitha H. Neesham-McTiernan, mailto:talimctiernan@arizona.edu

warming, increasing to 15% under the +4 °C scenario (Fan & McColl, 2024). Without effective interventions to reduce heat exposure in agricultural settings, both worker safety and global food production face unprecedented threats.

Agrivoltaic systems (Dupraz et al., 2011; Zastrow & Goetzberger, 1982), which integrate solar electricity production with agriculture, may offer an innovative adaptation strategy by modifying the thermal environment experienced by farmworkers. Although much agrivoltaic research has centered on system optimization (Arena et al., 2024; P. Campana et al., 2021; Hackenberg et al., 2023; Katsikogiannis et al., 2022; Kim & Kim, 2023; Mohseni & Brent, 2024; Riaz et al., 2021; Si et al., 2024), crop production (AL-agele et al., 2021; Amaducci et al., 2018; Barron-Gafford et al., 2019; Gonocruz et al., 2021; Lopez et al., 2023; Ludzuweit et al., 2025; Mohammedi et al., 2023; Rouini et al., 2025; Sekiyama & Nagashima, 2019; Thompson et al., 2020; Weselek et al., 2021), and land-use efficiency (Andrew et al., 2021; P. E. Campana et al., 2024; Giri & Mohanty, 2022; Ravishankar et al., 2023; Sarr et al., 2023; Trommsdorff et al., 2021; Valle et al., 2017; F. Zhang et al., 2023; Zheng et al., 2021), many studies have also documented significant modifications to air temperature, wind speed, humidity, and solar radiation. These four variables govern heat exchange and therefore collectively control environmental heat exposure (Bröde et al., 2012; Budd, 2008; Cheng et al., 2012; Gao et al., 2018; Jacobs et al., 2019; Liu et al., 2023; Middel & Krayenhoff, 2019; Minard et al., 1957). The concurrent impact of agrivoltaics on all four variables thus may offer unexamined benefits for reducing farmworkers heat exposure.

How effectively agrivoltaic systems reduce farmworker heat exposure depends on the extent to which they modify each of these four variables. Air temperature effects show mixed results with many studies reporting reductions, ranging from 0.5-4.2 °C in agrivoltaic systems during peak daytime hours (AL-agele et al., 2021; Armstrong et al., 2016; Ashraf Zainol Abidin et al., 2024; Barron-Gafford et al., 2019; Disciglio et al., 2023; Moon & Ku, 2022; Thum et al., 2025; Weselek et al., 2021; F. Zhang et al., 2023), while others find no significant difference (Fagnano et al., 2024; Marrou, Wery, et al., 2013). Wind speed, though studied less frequently than air temperature, typically decreases, with reductions of up to 38% reported (Adeh et al., 2018; Ahn et al., 2022; AL-agele et al., 2021; Fagnano et al., 2024), whereas humidity generally increases (Adeh et al., 2018; AL-agele et al., 2021; Ashraf Zainol Abidin et al., 2024; Barron-Gafford et al., 2019; Juillion et al., 2024; Moon & Ku, 2022; Othman et al., 2023). The most consistent environmental modification reported across studies is reduced solar radiation (Barron-Gafford et al., 2019; Carreño-Ortega et al., 2021; Disciglio et al., 2025; Gonocruz et al., 2021; Hudelson & Lieth, 2021; Kavga et al., 2018; Lopez et al., 2024; Marrou, Guilioni, et al., 2013; ?, ?; Mohammedi et al., 2023; Moon & Ku, 2022; Mupambi et al., 2022; Rouini et al., 2025; Valle et al., 2017; Weselek et al., 2021; F. Zhang et al., 2023; Zheng et al., 2021)

The consistency of solar radiation reduction across studies is significant given the critical role radiation plays in determining outdoor heat stress (Blazejczyk et al., 1993; Fan & McColl, 2024; Hwang & Lin, 2007; Nelson et al., 2024; Nielsen et al., 1988; Otani et al., 2016; L. Zhang et al., 2020). Research demonstrates that exposure to direct sunlight can reduce physical work capacity by up to 20% compared to shaded conditions (Foster et al., 2022), with life-threatening heat exposure up to 25 times higher when radiation is factored in (Fan & McColl, 2024). Despite the capacity of shade to reduce mean radiant temperature by 20-40 °C in various climates worldwide (Johansson & Emmanuel, 2006; Kantor et al., 2018; Middel et al., 2021), agricultural settings often lack consistent shade protection for workers (Kearney et al., 2016). The substantial reductions in solar radiation provided by agrivoltaics, combined with the modest air temperature decreases reported in many studies, suggest these systems could offer significant thermal benefits for farmworkers. However, the combination of increased humidity and reduced wind speed could potentially offset these benefits, particularly in environments where evaporative cooling is already compromised (Chow et al., 2016). Given these competing effects, re-

search directly assessing the combined impact of these four environmental variables is needed to understand how these systems might impact the health of those working within them. Further, as agrivoltaic systems continue to expand (Lepley et al., 2025; Magarelli et al., 2024; Weselek et al., 2019), with installations accelerating globally and workers already operating under them, it is crucial to determine their net impact on farmworker heat exposure, both to ensure new systems are designed with worker protection in mind and to mitigate any thermal hazards in existing systems.

To determine whether agrivoltaics can reduce farmworker heat exposure, we compared thermal conditions between traditional full sun agriculture and the two of the most common forms of agrivoltaic system: overhead (photovoltaic panels directly over agriculture) and interspaced (rows of photovoltaic panels interspaced with agriculture). Since panel density and mounting heights are two primary design considerations in agrivoltaic systems, our treatments included 50% and 100% panel coverage (overhead system) and 1.8 m and 2.4 m panel heights (interspaced system). Using multi-year empirical microclimate data collected from two sites in the southwestern United States, we quantified all four environmental variables that govern thermal stress and, uniquely among agrivoltaic studies, directly measure globe temperature, a measure of radiant heat from the sun and surrounding surfaces, in these systems. Using these empirical measurements as model inputs, we calculate Wet Bulb Globe Temperature (WBGT), a measure of human heat stress in direct sun, across peak (June-August) and shoulder (April-May, September-October) growing seasons to quantify differences in heat exposure experienced by workers in agrivoltaic systems versus full sun conditions. This analysis directly addresses the question: can agrivoltaics reduce the heat exposure experienced by outdoor farmworkers?

Methodology

Study sites and experimental design

We quantified heat stress differences between agrivoltaic systems and full-sun controls at two research sites in the southwestern United States. Each site featured two distinct agrivoltaic configurations, enabling comparative analysis across four agrivoltaic treatments and their corresponding full-sun control plots. The four agrivoltaic treatments are as follows: 1) overhead system with 100% panel coverage (data period 2020-2022), 2) overhead checkered board with 50% panel coverage (data period 2022-2025), 3) interspaced system with 1.8 m panel mounting height (data period 2022-2025), and 4) interspaced system with 2.4 m panel mounting height (data period 2022-2025). Control site data span the same time periods as their respective treatments.

Overhead system description

The overhead system known as the Biosphere 2 (B2) agrivoltaics learning lab is located near Tucson, AZ, USA (32.578989 °N, 110.851103 °W, elevation 1,381 m) in a hot semi-arid climate (Köppen BSh; (Kottek et al., 2006)) characterized by extreme summer heat, with mean maximum temperatures exceeding 38°C, soil temperatures exceeding 50°C, and limited annual precipitation (<30 cm). The agrivoltaics system consists of south facing fixed tilt (32°from horizontal) panels mounted with their lower edge 3.3 m above ground. Originally the system had 72 panels (each 0.83 m x 1.9 m tall) arranged in six east-west oriented rows of 12 solar panels within a 12.25 m x 14 m footprint. On September 28th, 2022, we modified the array by removing alternating panels in a checkerboard pattern, creating a temporal comparison between dense (100% coverage) and sparse (50% coverage) shading treatments (Supplementary Figure 1). As noted in previous studies from this site, the original system design (100% coverage) had an approximate ground coverage ratio of 0.75((Rouini et al., 2025)), as such it is important to note that the 100% coverage refers to 100% of the original panels, however this does not equate to a ground

coverage ratio of 1.0. Similarly, 50% coverage refers to 50% of the original panels, and not a ground coverage of 0.5. An adjacent full-sun control area of equal size provides reference conditions for both the 100% and 50% panel coverage treatments. The site cultivates research crops that change annually based on research objectives.

Interspaced system description

The interspaced system known as Jacks' Solar Garden (JSG) is a 1.2 MW community solar garden in Longmont, Colorado, USA (40.121917°N, 105.130528°W, elevation 1508 m) experiencing a cold semi-arid climate (Köppen BSk; (Kottek et al., 2006)) with hot summers and temperatures regularly exceeding 32°C, cold winters with January minimum temperatures averaging -6°C, and seasonal precipitation averaging 33.8 cm annually. The site contains 3,276 north-south oriented panels (2 m x 1 m) on a single axis tracking system that tracks east-west, rotating from maximum tilt (45°) eastward at sunrise to minimum tilt (-45°) westward at sunset, lying flat at midday and at night. The installation included panels at two mounting heights, 1.8 m (6 foot) in the western section and 2.4 m (8 foot) in the eastern section, with panel rows spaced 3.2 m apart in both sections (Supplementary Figure 2). A full sun control area is located south of the array. The site operates both as a research facility and non-profit production farm, cultivating food crops for both research and local distribution.

Measurement of environmental variables

Data collection

Micrometeorological stations were installed in control and each of the agrivoltaic treatments. Environmental variables were measured at 30-minute intervals, with each recorded value representing the average of the preceding 30-minute measurement period. At the overhead site, air temperature and relative humidity sensors (HMP45/HMP60, Campbell Scientific with radiation shield) and photosynthetically active radiation (PAR) sensors (LI-190R, LI-COR) were deployed at 2 m in the control area and at both 0.5 m and 2 m in the agrivoltaic treatment (note: we analyzed the 2 m agrivoltaic data to match the control, except for PAR where we use the average between the 0.5 m and 2 m sensors to better match the radiation patterns hitting the black globe sensor. Supplementary Figure 3 shows 2 m vs 0.5 m air temperature and humidity comparisons). Wind speed (RM Young 05103) and black globe temperature sensors (Campbell Scientific, 15.2 cm diameter) were added later (May 2024) at 1.5 m and 1.25 m respectively in control and 50% coverage. These measurements were not available for the 100% coverage period (2020-2022) as the sensors were installed after the panel modification. At the interspaced site, air temperature, relative humidity, and PAR sensors were installed at 0.75 m in the agrivoltaic treatments and the control condition. Black globe temperature sensors were installed (June 2023) at 1.5 m in all treatments. Wind speed was measured at 1.5 m in control and the 1.8 m treatment, but was not available for 2.4 m.

Data processing and quality control

Data quality control procedures included the removal of physically impossible values, detection and removal of statistical outliers and identification of sensor malfunction periods. Wind speed data gaps for both sites were reconstructed using random forests (details below). Air temperature, humidity, PAR and globe temperature were not gapfilled. Solar radiation was calculated from measured PAR using site-specific conversion factors accounting for site specific conditions (details below). Finally, globe temperature was modeled for the historical period at the overhead site when the input data was available (model details below).

Solar radiation calculation

Solar radiation was calculated from measured PAR using site-specific conversion factors accounting for altitude conditions. PAR measurements were first converted from μmol s^{-1} m^{-2} to W m^{-2} using the standard conversion factor of 0.217 W·m^{-2} (μmol s^{-1} m^{-2}) (Thimijan and Heins, 1983). Solar radiation was then derived using site specific PAR to Solar radiation ratios: 0.50 for the interspaced site (1526 m elevation) and 0.47 for the overhead system (1381 m elevation). These ratios account for reduced atmospheric attenuation of solar radiation at higher altitude, where decreased atmospheric mass and water vapor content result in higher PAR transmission relative to total solar radiation compared to standard sea-level conditions (Proutsos et al., 2022). Calculated solar radiation values from control treatments were validated against measured nearby meteorological stations to ensure accuracy.

Wind speed reconstruction

Wind speed data was not available for the complete study period at both sites and was reconstructed based on relationships between site measurements (interspaced system) and external meteorological stations (overhead system) during overlapping periods. The reconstruction was done with random forest regression models. For the overhead system, 80% of the wind speed data was reconstructed by establishing the relationship between data from a nearby meteorological station and measured wind speeds in 50% coverage and control during overlapping periods. The models incorporated temporal features, lagged wind speed values, and rolling statistics. Models were trained on 80% of the data (one model per treatment), and yielded a score of $R^2 = 0.73$, RMSE = 0.34 m/s for 50% coverage, and $R^2 = 0.74$, RMSE = 0.38 m/s for control on the test set (20% of the data). The trained models were then used to predict wind speeds from the weather station measurements for the missing time steps. Wind speed reconstruction was not possible for 100% coverage because no wind speed measurements were collected during this time period. Consequently, a direct relationship between the external wind speed data and 100% coverage wind speed could not be established. Where wind speed data was needed as an input for the WBGT model (see below), we applied the relationship derived from the 50% coverage period to estimate 100% wind speed. Given that panel modifications occurred at 3.3 m height while wind measurements were at 1.5 m (suggesting minimal impact on near-surface conditions), this substitution represents a limitation as some differences in wind patterns between coverage periods cannot be ruled out. For the interspaced site, no external weather station was available, and wind speed was reconstructed using bidirectional Random Forest models that used the spatial correlation (r = 0.81) between the control and 1.8 m treatment during their overlapping measurement periods (25,023 paired observations representing 70% temporal overlap). Missing 1.8 m wind speed was predicted from control data (test score on 20% of the data of $R^2 = 0.73$, RMSE = 0.36 m/s), while missing control wind speed was predicted from 1.8 m measurements (test score on 20% of the data of $R^2 = 0.84$, RMSE = 0.38 m/s). Similar to the 100% coverage, wind speed reconstruction was not possible for 2.4 m treatment as no wind speed sensor was installed in this section. Where wind speed was required, the 1.8 m wind speed data was used. This substitution represents a limitation as wind patterns may differ between 1.8 m and 2.4 m mounting heights due to differences in panel height and potential changes in airflow patterns.

Heat stress assessment

Wet Bulb Globe Temperature calculation

We calculated Wet Bulb Globe Temperature (WBGT) as our heat stress metric because it integrates all four of the primary drivers of outdoor thermal conditions and is used internationally as a tool for determining safe working conditions in sport, mil-

itary, and other outdoor labor (Budd, 2008; Parsons, 2006; Wyndham & Atkins, 1968). WBGT is calculated using the formula:

$$WBGT = 0.7\ T_{nwb} + 0.2\ T_g + 0.1\ T_a, \tag{1}$$

where T_{nwb} is natural wet bulb temperature, T_g is globe temperature, and T_a is air temperature (all in °C). To calculate WBGT, we used measured T_a for all treatments, only measured T_g was used for the interspaced treatments, whilst T_g was modelled at the overhead site to extend the measurement record. T_{nwb} was modelled for all treatments. To model T_g and T_{nwb} we used a modified version of the Liljegren et al. (2008) model, which is widely regarded as being the most accurate model for estimating WBGT from standard meteorological inputs (Patel et al., 2013). The model calculates T_g and T_{nwb} from the following inputs: air temperature, relative humidity, wind speed, solar radiation, barometric pressure, and solar zenith angle. Barometric pressure measurements were available for the overhead site from an onsite meteorological station, while a constant barometric pressure was used for the interspaced site based on local data records. Solar zenith angles were calculated using the pysolar library (Reda & Andreas, 2008), based on site coordinates and timestamps. For the control condition at the overhead site, we implemented the standard Liljegren model for globe temperature with two small modifications to prevent computational instabilities while preserving the original physics. We (1) capped solar zenith angle (capped to 85°zenith angle, corresponding to cos $\theta = 0.0872$) to prevent division by zero in the solar term during the day, and (2) tightened the exponential bounds (±4 vs. unlimited) in the direct/diffuse fraction calculation to prevent numerical overflow. For the agrivoltaic treatments, we modified the Liljegren globe temperature model more extensively to account for the altered radiation environment under the solar panels. These modifications changed the radiation environment from a "globe under open sky" to a "globe under/close to heated solar panels" which was achieved through four modifications.

The standard Liljegren model assumes globe sensors receive longwave radiation from the atmosphere only:

$$LW_{atm} = {}^1\!/_2\,(1 + \varepsilon_a) \cdot \sigma \cdot T_a^4, \tag{2}$$

where LW_{atm} is atmospheric longwave radiation, ε_a is the emissivity of the atmosphere, $\sigma = 5.67 \times 10^{-8}$ W m^{-2} K^{-4}, the Stefan-Boltzmann constant. Note that T_a is here in Kelvin.

However, agrivoltaic installations create fundamentally different radiative environments where heated solar panels block exchange with the atmosphere and represent a longwave source. We replaced the atmosphere only equation with a weighted multi-source model:

$$LW_{net} = V_{sky} \cdot F_{sky} + V_{panel} \cdot F_{panel}, \tag{3}$$

where LW_{Net} is the net longwave radiation from the environment to the globe (W m^{-2}). V_{sky} and V_{panel} are dimensionless view factors (0-1) representing the fraction of the globe's hemispherical view occupied by the sky and panels, respectively, with $V_{sky} + V_{panel} = 1$. F_{sky} is the flux from the sky (W m^{-2}). F_{panel} is the flux from the panels (W m^{-2}). Sky radiation (F_{sky}) was calculated using the Liljegren atmospheric model (equation 2); however, for ε_a, we used the Martin-Berdahl clear sky emissivity model instead of the standard vapor pressure-based emissivity, where:

$$\varepsilon_a = 0.711 + 0.0056 \cdot T_{dp} + 0.000073 \cdot T_{dp}^2 + \ 0.013 \cdot \cos\left(15\,(T_a - T_{dp})\right), \tag{4}$$

where ε_a is the clear sky emissivity and T_{dp} is dew point temperature calculated from air temperature and relative humidity using the Magnus-Tetens formula(Tetens, 1930). Panel radiation (F_{panel}) was calculated from panel surface temperatures:

$$F_{panel} = \sigma \cdot \varepsilon_{panel} \cdot T_{panel}^4, \tag{5}$$

where $\varepsilon_{panel} = 0.85$ (panel emissivity), and T_{panel} is the calculated panel surface temperature (K) using enhanced SAM/NOCT methodology. View factors for sky (V_{sky}) and panel (V_{panel}) radiation exchange were calculated using geometric analysis with the pyviewfactor library based on actual panel dimensions, spacing, height, and tilt angle. Static view factors were calculated for 100% panel coverage ($V_{sky} = 0.298$, $V_{panel} = 0.702$), 50% panel coverage ($V_{sky} = 0.543$, $V_{panel} = 0.457$).

Since panels become heat sources in the modified radiative environment, accurate panel temperature estimation is critical for longwave radiation calculations. We developed a dual-phase panel temperature model using the System Advisor Model (SAM) photovoltaic performance model (Gilman et al., 2018), which includes the Nominal Operating Cell Temperature (NOCT) methodology for daytime calculations and thermal mass physics for nighttime calculations. The daytime model uses an iterative energy balance where heat generated (Q_{heat}) equals heat loss (Q_{loss}). Heat generation:

$$Q_{heat} = G_{solar} \cdot a_{solar} \cdot (1 - \eta_{electrical}) \,. \tag{6}$$

Where G_{solar} is incident solar irradiance (W/m2), a_{solar} is solar absorptance (0.95 initially, degraded 0.4%/year), and $\eta_{electrical}$ is electrical conversion efficiency. Heat loss:

$$Q_{loss} = h_{conv} \left(T_{panel} - T_{air}\right) + h_{rad} \left(T_{panel} - T_{sky}\right) \tag{7}$$

Where h_{conv} is the convective heat transfer coefficient in W m-2 K-1 ($h_{conv} = 2.8 + 3.0 \cdot v_{wind}$, where 2.8 represents natural convection baseline (W m-2 K-1), 3.0 is the forced convection coefficient per unit wind speed, and v is wind speed in m/s adjusted from control measurement height to panel height using a logarithmic wind profile with surface roughness), h_{rad} is the radiative heat transfer coefficient using Martin-Berdahl sky temperature (W m-2 K-1), T_{panel} is panel surface temperature in Kelvin, and T_{sky} is effective sky temperature from the Martin-Berdahl model (K). The iterative energy balance is solved until panel temperature converges within 0.1 °C between iterations. The nighttime model incorporates thermal mass effects using principles for exponential cooling. The energy balance, which represents thermal storage rate being equal to heat loss rate, is as follows:

$$T_{panel} = T_a + \Delta T_{thermal} \cdot exp\left(-\Delta t / \tau\right) \tag{8}$$

Where t is thermal time constant (seconds) ($C_{thermal} / \left(h_{conv} + h_{rad}\right)$), $C_{thermal}$ is 20,000 J/m^2/K (heat storage capacity per unit panel area), Δt is the measurement interval (1800 seconds), $\exp(-\Delta t/\tau)$ is the retention factor representing exponential cooling, and $\Delta T_{thermal}$ is the retained heat above air temperature.

We used control solar radiation as unblocked radiation (G_{solar}) for solar panel heating calculations, and agrivoltaic solar radiation was used for the globe solar term. This reflects that panels receive full solar radiation while the globe sensors receive reduced irradiance due to panel shading. For natural wet bulb temperature calculations, we applied the original Liljegren model without modification for control and agrivoltaic treatments, as the wick evaporation physics are primarily controlled by air temperature, humidity, and wind speed rather than radiative environment. While overhead panels may have minor effects on the wet bulb radiative environment, these are expected to be minimal compared to the large radiative changes affecting globe temperature, and treatment differences are likely adequately captured through the measured meteorological inputs.

Globe temperature model validation

Both the control and overhead agrivoltaic globe temperature model were validated against measured black globe temperature from the field sensors. The control model performed well against control treatment observations: RMSE = 1.12°C, MAE = 0.82°C, $R^2 = 0.993$, bias = -0.28 °C (Supplementary Figure 4, 5), demonstrating that the model accurately captures globe temperature dynamics in the full sun. The agrivoltaic model

was similarly validated against the globe temperature observations from the 50% coverage treatment (RMSE = 2.16 °C, MAE = 1.31 °C, R^2 = 0.962, bias = 0.18 °C [Supplementary Figure 6, 7]). Model errors were primarily attributed to temporal offsets in diurnal peaks and troughs rather than systematic bias, resulting from spatial separation between meteorological input sensors and the globe temperature sensor within the treatment. Time series analysis revealed that the model accurately captured daily patterns, seasonal variation, and temperature magnitudes, with discrepancies largely manifesting at phase shifts of 30-60 minutes rather than amplitude error (Supplementary Figure 7). This indicated the model correctly represents the underlying physics, with remaining errors attributable to micro-spatial variations in input data rather than fundamental model limitations. Globe temperature sensors were not available for the 100% coverage treatment, meaning this treatment could not be directly validated. However, the model framework was validated using the 50% coverage treatment, which represents the same physical environment and panel configuration as 100%, but with fewer panels. Since our model accounts for panel density differences through the sky view factor calculations (V_{sky} and V_{panel}), the successful validation at 50% coverage provides confidence in the model's ability to accurately represent the 100% coverage radiative environment.

WBGT validation

To further validate our analysis, we compared modeled WBGT values against observed WBGT measurements from field instruments (Kestrel 5400 Heat Stress Tracker) collected during limited field campaigns at both study sites. At the overhead site, model validation for the 50% coverage treatment and its respective control showed model bias of -0.81 °C and -1.23 °C, respectively, with strong correlations (R^2 = 0.915 and 0.970) and RMSE values of 1.47°C and 1.57°C (Supplementary Figure 8). At the interspaced site, model validation for the 1.8 m treatment and control yielded model bias of -0.67 °C and -0.94°C, respectively, with strong correlations (R^2 = 0.934 and 0.952) and RMSE values of 1.78 °C and 1.27 °C (Supplementary Figure 9). Previous validation studies of the Kestrel Heat Stress Tracker (model 4400) instruments have shown they tend to overestimate WBGT in prolonged direct sunlight and low wind speed, with reported instrument uncertainty of 1.23 °C RMSE (Cooper et al., 2017); "Kestrel 5400 WBGT heat stress tracker (HST) & weather meter," 2025) . The consistent pattern of negative bias in our models, with greater underestimation in higher sunlight and lower wind conditions at both sites, aligns with expected Kestrel overestimation behavior. Our RMSE values falling within or only modestly exceeding known instrument uncertainty, and the strong correlations across all treatments demonstrate that our models accurately capture diurnal patterns and treatment differences, providing confidence in our modeling approach and conclusions.

WBGT flag exceedance analysis

WBGT values were classified into standardized heat stress flags representing work/rest guidelines: white flag (25.6-27.7 °C), green flag (27.8-29.4 °C), yellow flag (29.5-31.0 °C), red flag (31.1-32.1 °C), and black flag (≥32.2 °C), with progressively shorter allowable work periods. Flag exceedance analysis was performed on only timestamps common to both control and treatment conditions to ensure temporal compatibility. For each treatment-control pair, we calculated the count and percentage of times each treatments exceeded different flag thresholds, as well as the change in exceedances relative to control conditions.

Statistical analysis

Final dataset description

The final number of paired data points between each treatment and control for each variable were: air temperature (100% coverage: 38,363 pairs; 50% coverage: 26,606 pairs; 1.8 m: 20,095; 2.4 m: 20,095), relative humidity (100% coverage: 38,191 pairs; 50% coverage: 26,407 pairs, 1.8 m: 21,294, 2.4 m: 21,294), wind speed (50% coverage: 13,500; 1.8 m: 18,330 pairs), solar radiation (100% coverage: 27,832 pairs: 50% coverage: 26,068 pairs; 1.8 m: 21,255 pairs; 2.4 m: 21,255), and globe temperature (50% coverage: 13,500 pairs; 1.8 m: 18,019 pairs; 2.4 m: 18,019 pairs). The final output of paired WBGT data points between each treatment and control were: 100% coverage: 27,141 pairs; 50% coverage: 25,136 pairs; 1.8 m: 17,958 pairs 2.4 m: 17,958 pairs.

Analytical framework

We analyzed patterns across two seasonal periods: peak heat season (May-August) and shoulder seasons (March-April, September-October). Diurnal patterns were characterized across 24-hour cycles using 30-minute intervals (48-time bins per day). Treatment comparisons quantified microclimate changes by comparing each agrivoltaic treatment against its corresponding control and examining effects of design parameters: panel density (overhead site) and mounting height (interspaced).

Variables analyzed

Six variables were examined: air temperature, relative humidity, wind speed, solar radiation, globe temperature. And WBGT. For the first five variables, which also served as model inputs, statistics were calculated exclusively from measured sensor data, excluding any reconstructed wind speed or modeled globe temperature data. Only WBGT analysis incorporated modeled values (namely, reconstructed wind speed and modeled globe temperature where measurements weren't available).

Time period classification

Time periods were classified as daytime or nighttime using site-specific sunrise and sunset times derived from observed solar radiation. Daily sunrise and sunset were determined by identifying when solar radiation first exceeded 1 W m^{-2}, and when it dropped below 1 W m^{-2}. These daily values were then averaged by month to establish consistent monthly day/night classification periods. For the overhead system (Arizona, no daylight savings), monthly sunrises and sunsets ranged from 06:00-08:08 and 17:13-19:42 respectively. For the interspaced system (Colorado, with daylight saving time correction), times ranged from 07:00-08:53 and 17:53-21:30 respectively.

Statistical methods

Statistical analysis was restricted to timestamps where data were available for both control conditions and the respective agrivoltaic treatment simultaneously. For the overhead system where agrivoltaic treatments occurred at separate time periods, data were analyzed from common observations between control and 50% coverage and then separately for 100% coverage and control. In contrast, at the interspaced site where all three treatments co-existed, analysis was completed on common data across all three treatments. For each environmental variable, season and treatment combination, the following statistics were calculated: (1) half-hourly differences between treatment and control, (2) 24-hour mean values, (3) separate daytime and nighttime mean values, (4) the half hour period of maximum and minimum percentage difference between treatment and control. All comparative values were calculated as absolute differences and percentage dif-

ferences. Error bands in Figures 3-5 represent standard error of the mean calculated across all observations within each seasonal 30-minute time bin. Significance testing was performed for all input environmental variables (air temperature, relative humidity, wind speed, solar radiation [Supplementary Table 1]), and globe temperature [Figure 3; Supplementary Table 2] as well as for WBGT [Figure 4, 5; Supplementary Table 3]. For each variable-season combination, Mann-Whitney U tests were used to compare treatment and control measurements within each 30-minute time bin, as well as day and night categories within each season-variable combination. Rank-biserial correlation was calculated to measure effect size. To account for multiple comparisons across the 48-half hourly time bins, False Discovery Rate (FDR) correction using the Benjamini-Hochberg procedure was applied at $\alpha = 0.05$.

Results

Agrivoltaic panel coverage and height determine microclimate modifications

Overhead system

Both overhead treatments significantly reduced daytime air temperature (all relationships discussed $p \leq 0.01$ unless otherwise noted, see Supplementary Table 1), with reductions consistent across panel coverage and season. During peak season, both treatments reduced mean daytime air temperature by 1.5% (Figure 1a, 1d). However, 50% coverage had a greater maximum cooling of 6.7% at 07:30, compared to 5.3% for 100% coverage. Cooling effects diminished in absolute magnitude in the shoulder season but increased in relative terms (100%: 2.2%, 50%: 1.8%). Both treatments increased mean nighttime air temperature. Daytime relative humidity exceeded control conditions in both panel coverage treatments and seasons: 100% coverage was 7.5% higher than control during peak season (Figure 1b) and 50% coverage was 6.4% higher (Figure 1f). Nighttime humidity was lower in 100% coverage compared to control, with reductions of 3.2% and 5.1% during the peak and shoulder season, respectively. Solar radiation was substantially reduced in both treatments relative to control, averaging 86.7% less in 100% coverage (Figure 1c), and 64.7% lower in 50% during the peak season (Figure 1g). However, where 100% coverage maintained consistently low solar radiation throughout the day, 50% coverage oscillated between higher and lower solar radiation. Maximum differences between the agrivoltaic treatments and control were recorded at 12:00 (-93.5%) for 100% and 13:30 (-88.5%) for 50% coverage. In the shoulder season, solar radiation demonstrated very similar relationships to during the peak season. Average wind speed was lower in 50% coverage compared to control in both seasons (Figure 1e). Despite this, increased evening windspeed compared to control was recorded, showing maximum increases of 41.2% in the peak season. Wind speed was not available for 100% coverage.

Interspaced system

Mean daytime air temperature was reduced in both interspaced treatments compared to control, with peak season mean reduction of 1.8% in 1.8 m (Figure 2a) and 3.5% in 2.4 m (Figure 2e). Cooling increased during the shoulder season, with mean daytime reductions of 3.7% in 1.8 m and 6.4% in 2.4 m. Peak season maximum cooling occurred at 09:30 when 1.8 m was 10.9% cooler than control, while 2.4 m reached 10.4% below control at 10:00. Maximum cooling showed larger relative reductions during the shoulder season. Both treatments saw a midday increase in air temperature, however this was only significant in peak season for 1.8 m which reached up to 4.8% warmer at 13:30 compared to control. In the shoulder season, an insignificant warming of 3.4% was found in 1.8m, while 2.4 m remained cooler than control throughout the day. Both treatments remained more humid than control. Daytime humidity increases relative to control were almost identical between the treatments during the peak season (1.8 m: +5.8% [Figure

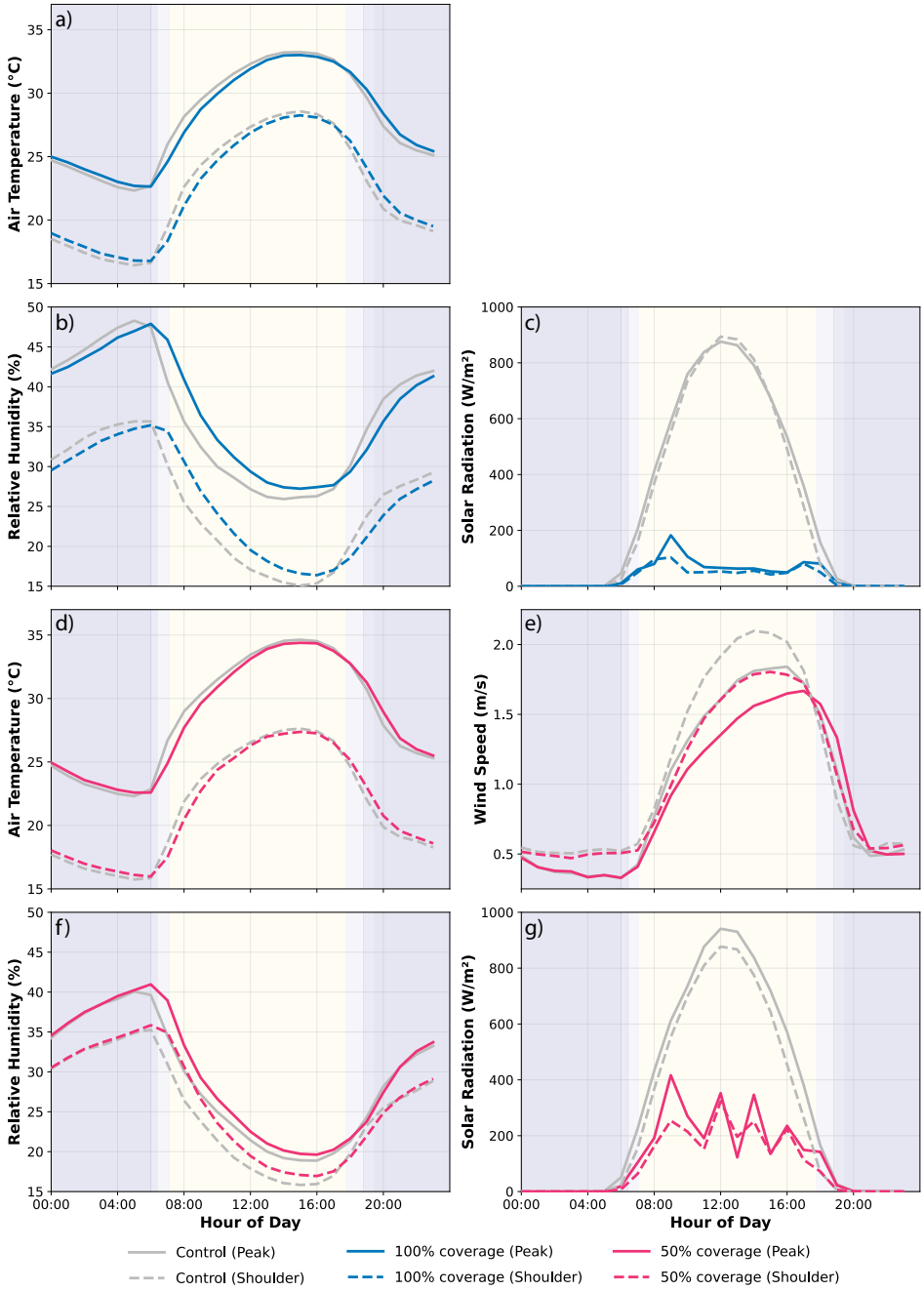

Figure 1: Diurnal patterns for the four thermal environmental variables under 100% and 50% panel coverage at the overhead agrivoltaic site during peak heat (June-August) and shoulder seasons (April-May, September-October). Air temperature (°C), wind speed (m/s), relative humidity (%), and solar radiation (W/m^2) are shown for 1) 100% panel coverage (Blue; before September 27, 2022) and 2) 50% panel coverage (pink; after September 27, 2022). Grey lines show full sun control conditions. Solid lines represent peak heat season, and dashed lines represent shoulder season. Yellow shading represents daytime, dark blue shading indicates nighttime, and gradient navy shows shifting sunrise and sunset times where darker gradients represent a given time is more often nighttime than daytime. Data points represent 30-minute averages calculated from all available common observations within each season and treatment.

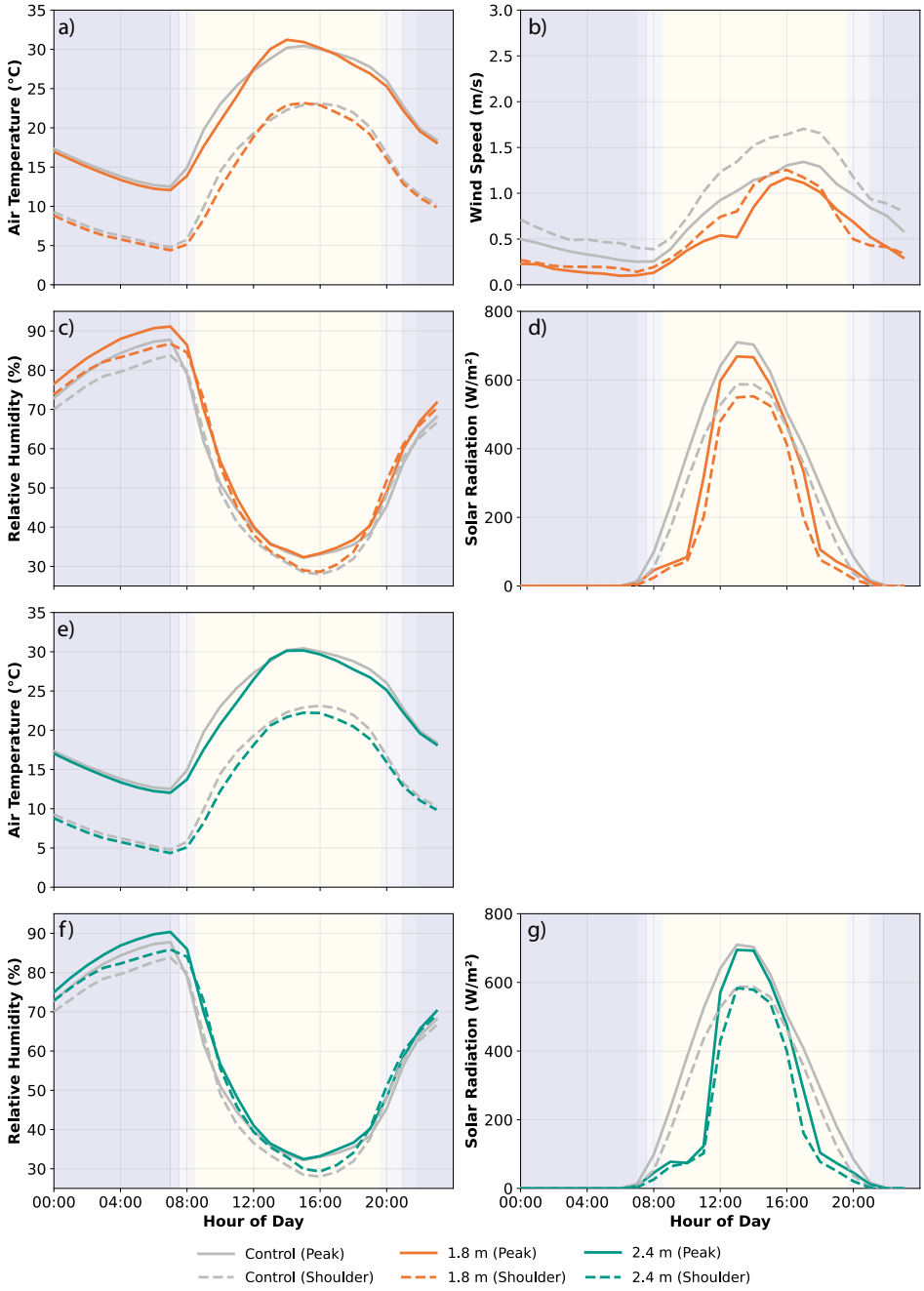

Figure 2: Diurnal patterns for the four thermal environmental variables measured in the 1.8m and 2.4m interspaced agrivoltaic systems during peak heat (June-August) and shoulder seasons (April-May, September-October). Air temperature (°C), wind speed (m/s), relative humidity (%), and solar radiation (W/m^2) are shown for 1) 1.8m height panels (orange) and 2) 2.4m height panels (green). Grey lines show full sun control conditions. Solid lines represent peak heat season and dashed lines represent shoulder season. Blue shading denotes average night while yellow shading denotes average daytime. Yellow shading represents daytime, dark blue shading indicates nighttime, and gradient navy shows shifting sunrise and sunset times where darker gradients represent a given time is more often nighttime than daytime. Data points represent 30-minute averages calculated from all available common observations within each season and treatment

2c], 2.4 m: +5.7% [Figure 2f]), whilst in the shoulder season 2.4 m was more humid (8.1% vs 6.8%). At night, 1.8 m stayed the most humid, +4.4% compared to +2.9% in 2.4 m. Solar radiation reduced more in the 2.4 m treatment (Figure 2g), with mean reductions of 28.2% compared to 24.7% in 1.8 m during the peak season (Figure 2d). Solar reduction peaked at 10:30 in 1.8 m but an hour later at 11:30 in 2.4 m, reducing by 78.2% and 72.2% respectively. Both treatments reduced morning solar radiation more than evening. Wind speed was 34% lower in 1.8 m during peak season (Figure 2b). The largest reduction was recorded at 13:30 when wind was 48.7% lower in 1.8 m than control, though nighttime showed greater relative reductions overall (53.2% vs 28% during daytime).

Agrivoltaics modify radiant heat loads experienced by farmworkers

Overhead system

50% coverage provided consistent globe temperature cooling from sunrise until late afternoon in both seasons (Figure 3a, Supplementary Table 2). Mean daytime globe temperature was 10.5% and 12.2% lower in 50% coverage compared to control during the peak and shoulder season, respectively. While both conditions followed a clear diurnal pattern, globe temperature in control rose and fell steadily whilst 50% coverage showed intermittent peaks and troughs resulting in mean globe temperature reductions of 16.5% at 12:00, but 4.7% at 14:00 (peak season). Maximum differences between control and 50% coverage were documented at 09:30, when 50% coverage was 17.7% cooler. In the shoulder season, maximum cooling reduced in absolute terms but represented a larger proportional cooling of 19.3% at 09:00. Globe temperature was on average 6.6% warmer in 50% coverage during the night during peak season, but 11.2% warmer during the shoulder season.

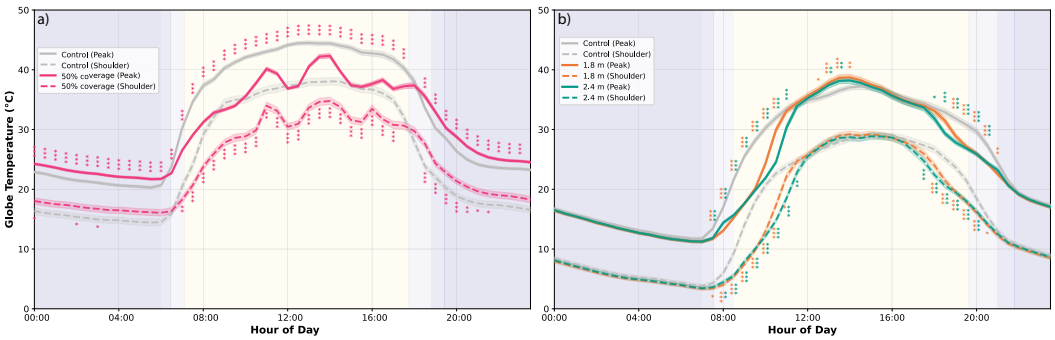

Figure 3: Diurnal globe temperature comparison between agrivoltaic treatments and control conditions during peak heat (June, July, August) and shoulder seasons (April, May, September, October) at the a) overhead agrivoltaic site, and b) interspaced agrivoltaic site. Grey lines represent control conditions, pink represents 50% panel coverage, orange represents 1.8 m panel height, and green represents 2.4 m panel height. Solid lines show peak heat season, while dashed lines indicate shoulder seasons. Statistical significance between control and the respective agrivoltaic treatment at each 30-minute timestep was determined using Mann-Whitney U with significance levels: * $p < 0.05$, ** $p < 0.01$, *** $p < 0.001$. Error bands show standard error of the mean. Yellow shading represents daytime, dark blue shading indicates nighttime, and gradient navy shows shifting sunrise and sunset times where darker gradients represent a given time is more often nighttime than daytime. Data points represent 30-minute averages calculated from all available common observations within each season and treatment

Interspaced system

The 2.4 m treatment reduced mean daytime globe temperature more than 1.8 m, and both showed afternoon warming despite overall daytime cooling (Figure 3b, Supplementary Table 2). During the peak season, mean daytime globe temperature was reduced by 5% in 1.8 m, and 7% in 2.4 m. The shoulder season showed larger daytime cooling, with mean reductions of 8.7% and 11%, respectively. Afternoon increases in globe temperature compared to control were greater in 1.8 m (+5.8%) and recorded 30 minutes later, at 13:30, compared to 2.4 m (+4.6%). Smaller midday increases of 3.8% and 2.8% were found during the shoulder season. These increases were balanced out by substantial cooling in the morning. At 09:30 in the peak season, 1.8 m was 28.8% cooler than control, whilst 2.4 m was 27.7% cooler. These maximum cooling differences increased in the shoulder season to 47% at 09:00 for 1.8 m and 44.2% at 09:30 for 2.4 m. Both treatments insignificantly reduced globe temperature during the nighttime.

Agrivoltaic microclimate modifications alter heat stress exposure

Overhead system

Wet bulb globe temperature (WBGT) was significantly reduced throughout the daytime in both treatments and seasons (Figure 4, Supplementary Table 3). 100% coverage remained on average 8.9% cooler than control during the peak season between the hours of 06:30 and 18:00 (Figure 4a). Comparatively, 50% coverage had a smaller cooling effect, reducing WBGT by 6.5% between 06:30 and 17:30 (Figure 4b). In the shoulder season, cooling increased, with WBGT an average of 12.9% lower in 100% between 07:00 and 17:30, and 9.1% lower than control in 50% for the 07:00-17:00 period. WBGT was always higher at night in both treatments compared to control, although this relationship reduced in significance after 22:30 in both seasons. 50% coverage had higher nighttime warming compared to 100%. WBGT is an international standard human heat index that can be categorized into six levels: unflagged (no restrictions) and five colored flags (white, green, yellow, red, and black) that represent progressively severe heat exposure thresholds requiring shorter work periods due to increased heat strain on the body (Budd, 2008, Parsons, 2006, patel2013). Substantial reductions in heat stress flag conditions requiring work restrictions were found in the overhead system compared to control, with 100% coverage reducing white flag or higher exceedances by 85% and 50% coverage reducing them by 52%.

Interspaced system

Both 1.8 m and 2.4 m reduced WBGT in the mornings but increased it during the afternoons (Figure 5, Supplementary Table 3). In peak season, 1.8 m was 10.2% cooler than control from 07:30-11:00 and 18:00-20:00, however, between 12:00-14:30 it was 6.8% warmer, with maximum warming reaching 9.9% higher than control (Figure 5a). 2.4 m had a larger cooling effect, reducing WBGT by 11.2% between 07:30-11:30 and 18:00-20:30. Afternoon warming was less in 2.4 m, increasing WBGT by 5.7% between 12:30-14:00, and reaching up to 7.4% warmer than control (Figure 5b). Both treatments had large morning cooling, with 1.8 m hitting 20% cooler than control, and 2.4 m peaking at 20.1% lower 30 minutes later at 10:00. In the shoulder season, afternoon warming was less prolonged and less significant, with a mean increase of 8.6% between 13:00-13:30 in 1.8 m. 2.4 m was not significantly warmer during the shoulder season. This meant mean daytime reductions in WBGT increased in the shoulder season. 1.8 m was 19.6% lower between 08:30-11:00 and 17:30-19:30, and 2.4 m was 20% between 08:30-11:30 and 17:00-19:30. Similarly, maximum reductions reached 34.6% and 33.1% respectively. Under both treatments and seasons, WBGT was insignificantly lower than control during the night. The increased afternoon WBGT in both treatments resulted in large increases in heat

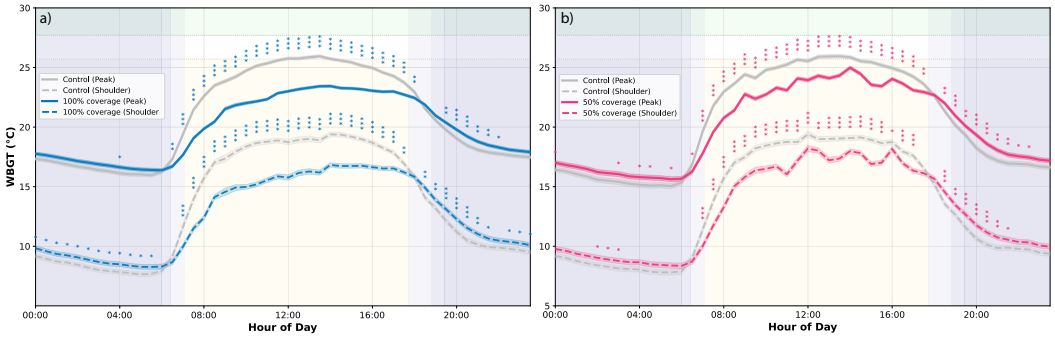

Figure 4: Diurnal patterns of Wet Bulb Globe temperature (WBGT) comparing full sun control and overhead agrivoltaics (AV) during peak heat season (June, July, August) and shoulder seasons (April-May, September-October). A) shows WBGT for the 100% panel coverage period (blue) and b) panel shows data from the 50% panel coverage period (pink). Solid lines show peak heat season, while dashed lines indicate shoulder seasons. Statistical significance between control and the respective agrivoltaic treatment at each 30-minute timestep was determined using Mann-Whitney U with significance levels: * $p < 0.05$, ** $p < 0.01$, *** $p < 0.001$. Error bands show standard error of the mean. Yellow shading represents daytime, dark blue shading indicates nighttime, and gradient navy shows shifting sunrise and sunset times where darker gradients represent a given time is more often nighttime than daytime. Colored horizontal bands across the top of each panel indicate WBGT heat stress categories: no band (< 25.5°C), white (25.6-27.7°C), and light green (> 27.8°C).

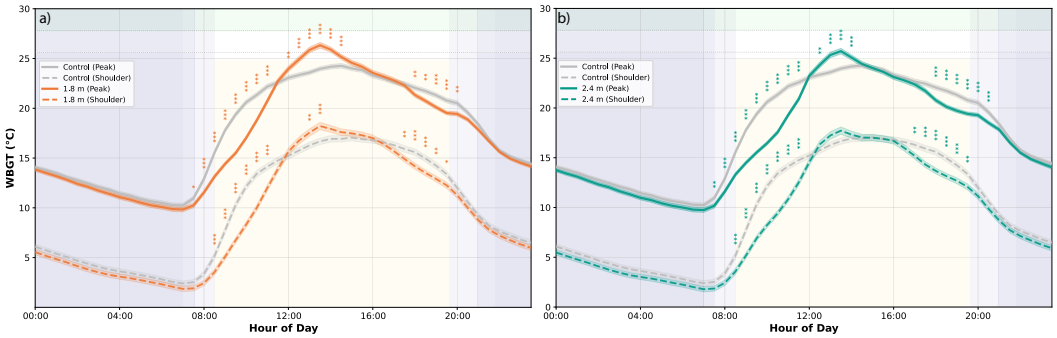

Figure 5: Diurnal patterns of Wet Bulb Globe temperature (WBGT) comparing full sun control and interspaced agrivoltaics (AV) during peak heat season (June, July, August) and shoulder seasons (April-May, September-October). A) shows the WBGT for the 1.8 m panel height treatment (orange) and b) shows the WBGT for the 2.4 m panel height treatment (green). Solid lines show peak heat season, while dashed lines indicate shoulder seasons. Statistical significance between control and the respective agrivoltaic treatment at each 30-minute timestep was determined using Mann-Whitney U with significance levels: * $p < 0.05$, ** $p < 0.01$, *** $p < 0.001$. Yellow shading represents daytime, dark blue shading indicates nighttime, and gradient navy shows shifting sunrise and sunset times where darker gradients represent a given time is more often nighttime than daytime. Colored horizontal bands across the top of each panel indicate WBGT heat stress categories: no band (< 25.5°C), white (25.6-27.7°C), and light green (> 27.8°C).

stress flag conditions, with 1.8 m increasing white flag or higher exceedances by 57% and 2.4 m increasing them by 17%.

Conceptual figure of agrivoltaic design effects on farmworker heat stress

The previously documented differences in air temperature, humidity, solar radiation, and wind speed (Figure 1 & 2) between treatments translate into measurably different thermal environments for farmworkers (Figures 4 & 5). Figure 6 synthesizes these microclimate modifications observed in our study, showing cooler conditions in both morning (Figure 2, 4, 6b) and early afternoon (Figure 4, 6e) in the overhead system compared to full sun control (Figure 4, 6a, 6d), whilst morning cooling (Figure 5, 6c) and early afternoon warming (Figure 5, 6f) is found in the interspaced system. This conceptual figure illustrates how agrivoltaic design choices directly influence heat exposure and thermal comfort throughout the working day.

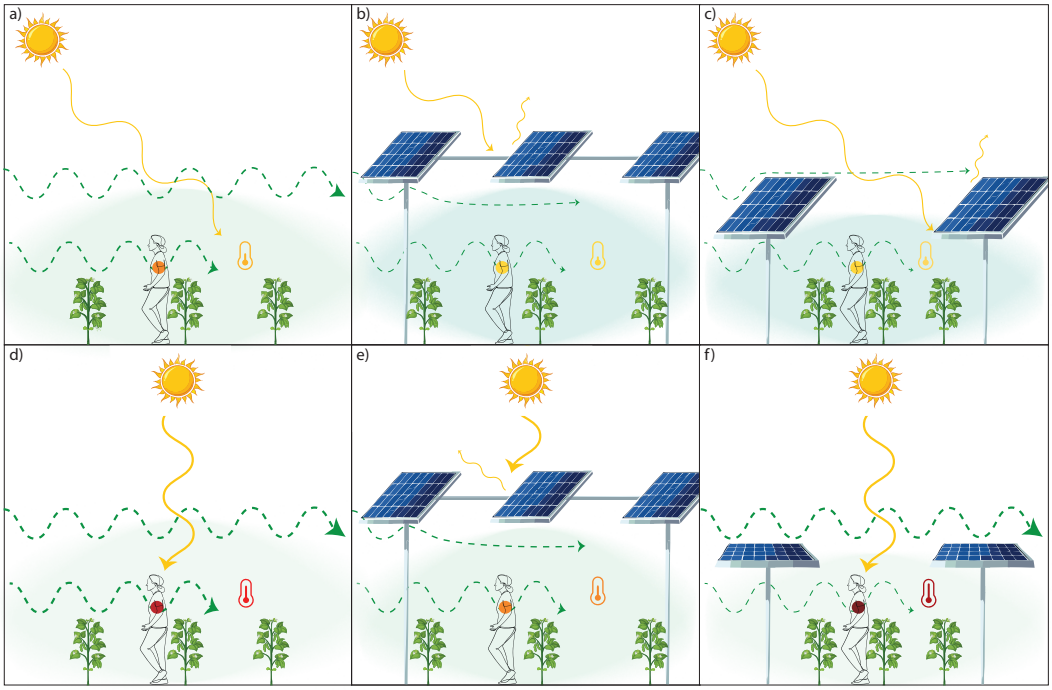

Figure 6: Conceptual figure describing changes in human thermal comfort between control (a, d), overhead agrivoltaics (b, e) and interspaced agrivoltaics (c, f). Yellow lines are solar radiation, and green dashed lines are wind speed. Thicker lines describe greater wind speed and solar radiation. Air temperature is represented by the thermometer symbol with yellow representing cooler conditions through to dark red representing hotter conditions. Relative humidity is represented by green/blue shading, with darker shading representing higher humidity. Colored circles within each person describes their human thermal comfort, with yellow representing cooler conditions and dark red representing hotter conditions. Sun position describes time of day, with the top row (a, b, c) illustrating morning, and the bottom row illustrating midday (d, e, f). The figure illustrates how overhead agrivoltaics provides consistently cooler environments throughout the workday compared to full sun agriculture, whilst interspaced agrivoltaics provided cooler morning conditions but increases midday to early afternoon heat.

Discussion

This study provides the first empirical evidence that agrivoltaics can significantly reduce heat exposure for farmworkers in semi-arid agricultural environments. Across both peak and shoulder seasons, all treatments showed mean daytime WBGT reductions compared to control, demonstrating overall heat mitigation benefits. However, these benefits varied in magnitude and timing according to system design. The overhead system yielded consistent protection throughout the day, particularly with higher solar panel density which provided almost continuous shading. 50% coverage delivered more variable shading, creating fluctuating cooling that peaked during shaded periods. Despite this oscillation, cumulative heat exposure in 50% coverage was much less than the corresponding control. Further, mobile farmworkers could maximize heat mitigation by moving with the shade, a potential benefit not captured by our static micrometeorological station. In contrast, the interspaced system reduced morning and evening heat exposure when lower solar angles created significant shading, but increased afternoon WBGT when the flattened panels exposed the inter-row beds to direct sun, eliminating shading benefits. The panels and mounting structure also reduced wind speed within the panel canopy, limiting convective cooling, resulting in increased heat exposure during critical midday hours. Importantly, this increase in afternoon heat was more severe and sustained under the lowest clearance (1.8 m) system, demonstrating intensifying heat risk as panel height decreased. These design differences have critical labor implications: overhead systems substantially reduced heat stress flags compared to full-sun, potentially offsetting climate-driven labor capacity losses, while interspaced systems (particularly low-clearance) increased flags, exacerbating predicted workforce reductions. However, strategic work scheduling in the interspaced systems could reduce heat exposure by avoiding midday periods. Our results highlight the potential of agrivoltaics to improve worker thermal comfort while demonstrating that system design choices are critical to thermal outcomes. As such, the health of farmworkers should be central to agrivoltaic system design.

The observed differences in cooling benefits between agrivoltaic treatments stem from their varied impact on the energy balance. Maximum reduction in environmental heat load occurs when the agrivoltaic system physically blocks sunlight and alters the partitioning of solar energy in agricultural settings. This reduces direct radiant heating, thereby lowering surface temperatures (Lopez et al., 2024; Weselek et al., 2021), air temperature (Barron-Gafford et al., 2019), and heat exposure (Middel & Krayenhoff, 2019). Overhead systems maximize this benefit by blocking sunlight during crucial solar maximum hours, ensuring at least partial shade when thermal conditions are most extreme. The reduced direct sunlight also slows evaporation, allowing water to remain in the system longer and prolonging evapotransporative cooling (Ashraf Zainol Abidin et al., 2024; Beniuga et al., 2025). This is particularly beneficial in high vapor pressure deficit climates where added moisture provides additional cooling without a problematic buildup in humidity. However, solar panels and mounting structures can impede airflow (Adeh et al., 2018; Ahn et al., 2022; Li & Sun, 2024), particularly when panels are mounted between ground and worker height (Bruhwyler et al., 2024), blocking wind where labor occurs and reducing convective cooling. When wind blocking is paired with little to no reduction in midday solar radiation, heat conditions can significantly worsen.

While the shading patterns and airflow dynamics described above were the dominant factors shaping heat exposure in our semi-arid environment, humidity represents an additional microclimate consideration that may become critical in other contexts. The modest increase in humidity observed in our agrivoltaic treatments did not exacerbate heat stress under the conditions examined. However, the combined effect of increased humidity and reduced wind speed should be carefully considered in agrivoltaic systems in more humid climates. In such climates, increased humidity coupled with decreased wind speed could compound heat stress by limiting convective alongside evaporative cooling, two of the body's primary heat dissipation mechanisms (Ferguson, 1988; Huang &

Zhai, 2020; Koop & Tadi, 2024; Koppe et al., 2004; Osilla et al., 2024), resulting in dangerous heat conditions (Budd, 2008; Platt & Vicario, 2013; Ravanelli et al., 2015). This consideration is critical given that humid-heat events are escalating globally (Bekris et al., 2023; Coffel et al., 2017; Hanna & Tait, 2015; Palmer, 2013; Poppick & McKinnon, 2020; Raymond et al., 2020; Willett & Sherwood, 2012). Such events pose a serious and growing threat to farmworker health and are linked to significant heat-related illness and death (Dally et al., 2020; Diaz et al., 2023; El Khayat et al., 2022; Fan & McColl, 2024; Flouris et al., 2018; Kang & Eltahir, 2018; Mishra et al., 2020; Mora et al., 2017; Spector et al., 2016). Therefore, examining agrivoltaic impacts on wind flow and humidity is crucial to avoid inadvertently contributing to the growing humid-heat risk faced by farmworkers.

These human safety considerations must be weighed against the plant-focused benefits that an agrivoltaic microclimate can provide. Research has demonstrated that the wind sheltering effect of agrivoltaics can increase crop yields (Honningdalsnes et al., 2025). Similarly, greater soil moisture retention and increased humidity can improve plant productivity (Adeh et al., 2018; Ashraf Zainol Abidin et al., 2024; Barron-Gafford et al., 2019; Marrou, Guilioni, et al., 2013), particularly when plants are heat-stressed (Amaducci et al., 2018; Disciglio et al., 2025). This highlights a fundamental trade-off between human- and plant- centric benefits of agrivoltaics whereby humid-heat is preferable for plant survival (Lesk et al., 2022; Schauberger et al., 2017; Ting et al., 2023; Troy et al., 2015) but dry-heat is preferable for human survival (Buzan & Huber, 2020; Gillett et al., 2021; Haldane, 1905; Hanna & Tait, 2015; Raymond et al., 2020; Rogers et al., 2021; Russo et al., 2017; Sherwood, 2018; Sherwood & Huber, 2010; Vecellio et al., 2022; Willett et al., 2007). From a crop-centric perspective, maximizing wind sheltering and humidity retention within an agrivoltaic system might be desirable to limit water stress. However, in a human-centric system the opposite would be true. Consequently, crop needs should be carefully considered in balance with the needs of those who work within the system to ensure crop productivity is maximized without compromising farmworker health.

The demonstrated heat mitigation potential of well-designed agrivoltaic systems is particularly significant given the escalating threat of heat exposure to farmworker health and agricultural productivity (de De Lima et al., 2021; El Khayat et al., 2022; Kjellstrom et al., 2016; Moda et al., 2019; Nelson et al., 2024; Simpson et al., 2021; Tigchelaar et al., 2020). Despite the urgency of this threat, many major agricultural regions lack robust heat protection legislation and practices, leaving farmworkers vulnerable to extreme heat exposure (Arnold et al., 2020; Courville et al., 2016; Irani et al., 2021). Where regulations do exist, they often focus on behavioral mitigation strategies, such as hydration, rest periods, access to shaded break areas, and protective clothing (Courville et al., 2016; Kearney et al., 2016). However, structural barriers, including piece-rate-pay systems that discourage breaks and the absence of guaranteed rest periods, can prevent workers from effectively implementing these protective behaviors (Edgerly et al., 2024; Morera et al., 2020; Spector et al., 2015). While behavioral strategies are essential (Day et al., 2019), they place the burden of heat mitigation on individual workers and may be insufficient under extreme or prolonged heat conditions (Langer et al., 2021). There is therefore a need for interventions that modify the thermal environment itself, moving beyond relying on worker behavior. Our findings demonstrate that agrivoltaics can provide such interventions, directly reducing heat load where farmwork occurs. However, design choices critically determine thermal outcomes. As shown here, lower mounting heights can worsen heat conditions during critical periods, potentially exacerbating rather than alleviating heat stress. If agrivoltaics are designed with worker thermal safety as a priority and integrated with behavioral heat mitigation strategies and policy protections, these systems could form a key component of an integrated approach to safeguarding farm labor in a warming world.

While this study provides multi-year evidence that agrivoltaics can reduce environmental heat exposure, its findings are based on four specific system configurations across two semi-arid locations. As such, results may not be generalized to other climates, particularly more humid or temperate regions where microclimate dynamics may differ. Further, the focus on environmental heat metrics as opposed to worker-reported experiences or physiological outcomes limits our ability to holistically assess the extent of occupational health impacts. Future research should extend to a wider range of climates, system designs, and labor contexts, incorporating worker-centered and physiological data. One promising avenue of future research is exploring dynamic tracking systems which could be programmed to prioritize heat protection for farmworkers during labor periods. While current tracking systems are typically programmed to prioritize electricity generation and sometimes crop productivity, a third strategy could program panels to maximize shading when and where farmworkers are actively laboring, shifting to crop or electricity optimized orientations during non-working hours. This temporal approach could substantially enhance worker protection during key heat exposure periods without compromising overall agricultural or electrical performance.

Advancing our understanding of the impact of agrivoltaics on human heat stress is essential in ensuring these systems are not only productive and scalable, but also safe and equitable under intensifying climate conditions. While agrivoltaics are often promoted as a win-win strategy across the water-energy-food nexus, achieving truly sustainable agricultural production requires centering the workforce that enables food systems. Moving forward, future agrivoltaic development should maximize benefits across energy, crop, and labor dimensions. Only through this integrated approach can agrivoltaics deliver on their promise as a climate solution for agriculture.

Acknowledgments

This research and data were supported by (1) the National Science Foundation Geography and Spatial Sciences through Award 2025727; (2) the National Renewable Energy Laboratory's InSPIRE project, through the U.S. Department of Energy Office of Energy (DOE) Efficiency and Renewable Energy Solar Energy Technologies Office under award DE-EE00034165; (3) the Kasser Joint Institute for Food, Water, and Energy Security; (4) the University of Arizona One Health Research Initiative, and (5) the Raphael and Jolene Gruener Research Travel Award. The authors thank the Biosphere 2 team for their assistance in maintenance of the Biosphere 2 Agrivoltaics Learning Lab monitoring systems, and the University of Arizona Biosphere 2 supported Landscape Evolution Observatory (LEO) Project for providing data. The authors would also like to thank Byron Kominek for access to Jack's Solar Garden and Amy Marble for maintaining the instrumentation at this site.

Data availability

Data will be made available in a public repository upon publication.

Declaration of competing interest

The authors declare that they have no known competing financial interests or personal relationships that could have appeared to influence the work reported in this paper.

References

Adeh, E. H., Selker, J. S., & Higgins, C. W. (2018, November). Remarkable agrivoltaic influence on soil moisture, micrometeorology and water-use efficiency.

PLOS ONE, *13*(11), e0203256. doi: 10.1371/journal.pone.0203256

Ahn, S., Lee, D.-B., Lee, H. I., Myint, Z., Min, S., Kim, B., ... Yun, H. (2022). Grapevine Growth and Berry Development under the Agrivoltaic Solar Panels in the Vineyards. *Journal of Bio-Environment Control*, *31*(4), 356–365. doi: 10.12791/ksbec.2022.31.4.356

AL-agele, H. A., Proctor, K., Murthy, G., & Higgins, C. (2021, January). A Case Study of Tomato (Solanum lycopersicon var. Legend) Production and Water Productivity in Agrivoltaic Systems. *Sustainability*, *13*(5), 2850. doi: 10.3390/su13052850

Amaducci, S., Yin, X., & Colauzzi, M. (2018, June). Agrivoltaic systems to optimise land use for electric energy production. *Applied Energy*, *220*, 545–561. doi: 10.1016/j.apenergy.2018.03.081

Andrew, A. C., Higgins, C. W., Smallman, M. A., Graham, M., & Ates, S. (2021, April). Herbage Yield, Lamb Growth and Foraging Behavior in Agrivoltaic Production System. *Frontiers in Sustainable Food Systems*, *5*. doi: 10.3389/fsufs.2021.659175

Arena, R., Aneli, S., Gagliano, A., & Tina, G. M. (2024). Optimal Photovoltaic Array Layout of Agrivoltaic Systems Based on Vertical Bifacial Photovoltaic Modules. *Solar RRL*, *8*(1). doi: 10.1002/solr.202300505

Armstrong, A., Ostle, N. J., & Whitaker, J. (2016, July). Solar park microclimate and vegetation management effects on grassland carbon cycling. *Environmental Research Letters*, *11*(7), 074016. doi: 10.1088/1748-9326/11/7/074016

Arnold, T. J., Arcury, T. A., Sandberg, J. C., Quandt, S. A., Talton, J. W., Mora, D. C., ... Daniel, S. S. (2020, August). Heat-Related Illness Among Latinx Child Farmworkers in North Carolina: A Mixed-Methods Study. *NEW SOLUTIONS: A Journal of Environmental and Occupational Health Policy*, *30*(2), 111–126. doi: 10.1177/1048291120920571

Ashraf Zainol Abidin, M., Faqihah Jamrus, N., Iman Azman, N., Illani Abdul Razak, N., & Faezah Omar, N. (2024, December). Evaluating the Impact of Agrivoltaic Systems on Microclimate and Andrographis paniculata Growth. *IOP Conference Series: Earth and Environmental Science*, *1426*(1), 012013. doi: 10.1088/1755-1315/1426/1/012013

Barron-Gafford, G. A., Pavao-Zuckerman, M. A., Minor, R. L., Sutter, L. F., Barnett-Moreno, I., Blackett, D. T., ... Macknick, J. E. (2019, September). Agrivoltaics provide mutual benefits across the food–energy–water nexus in drylands. *Nature Sustainability*, *2*(9), 848–855. doi: 10.1038/s41893-019-0364-5

Bekris, Y., Loikith, P. C., & Neelin, J. D. (2023). Short Warm Distribution Tails Accelerate the Increase of Humid-Heat Extremes Under Global Warming. *Geophysical Research Letters*, *50*(11), e2022GL102164. doi: 10.1029/2022GL102164

Beniuga, C. R., Pingescu, B. A., Beniuga, O. C., Dragomir, A., Astanei, D.-G., & Burlica, R. (2025, April). Photovoltaic Panel System with Optical Dispersion of Solar Light for Greenhouse Agricultural Applications. *AgriEngineering*, *7*(4), 125. doi: 10.3390/agriengineering7040125

Blazejczyk, K., Nilsson, H., & Holmér, I. (1993, September). Solar heat load on man. *International Journal of Biometeorology*, *37*(3), 125–132. doi: 10.1007/BF01212621

Bröde, P., Fiala, D., Błażejczyk, K., Holmér, I., Jendritzky, G., Kampmann, B., ... Havenith, G. (2012, May). Deriving the operational procedure for the Universal Thermal Climate Index (UTCI). *International Journal of Biometeorology*, *56*(3), 481–494. doi: 10.1007/s00484-011-0454-1

Bruhwyler, R., Brunet, P., Dabadie, G., Drahi, E., Souquet, P., Chapon, J., ... Lebeau, F. (2024, February). Could Windbreak Effect Significantly Decrease Evapotranspiration in Vertical Agrivoltaics? In *Agrivoltaics World Conference*

2022. TIB Open Publishing, Germany. doi: 10.52825/agripv.v1i.540

Budd, G. M. (2008, January). Wet-bulb globe temperature (WBGT)—its history and its limitations. *Journal of Science and Medicine in Sport*, *11*(1), 20–32. doi: 10.1016/j.jsams.2007.07.003

Buzan, J. R., & Huber, M. (2020, May). Moist Heat Stress on a Hotter Earth. *Annual Review of Earth and Planetary Sciences*, *48*(Volume 48, 2020), 623–655. doi: 10.1146/annurev-earth-053018-060100

Campana, P., Stridh, B., Amaducci, S., & Colauzzi, M. (2021, November). Optimisation of vertically mounted agrivoltaic systems. *Journal of Cleaner Production*, *325*, 129091. doi: 10.1016/j.jclepro.2021.129091

Campana, P. E., Stridh, B., Hörndahl, T., Svensson, S.-E., Zainali, S., Lu, S. M., ... Colauzzi, M. (2024, January). Experimental results, integrated model validation, and economic aspects of agrivoltaic systems at northern latitudes. *Journal of Cleaner Production*, *437*, 140235. doi: 10.1016/j.jclepro.2023.140235

Carreño-Ortega, A., do Paço, T. A., Díaz-Pérez, M., & Gómez-Galán, M. (2021, December). Lettuce Production under Mini-PV Modules Arranged in Patterned Designs. *Agronomy*, *11*(12), 2554. doi: 10.3390/agronomy11122554

Cheney, A. M., Barrera, T., Rodriguez, K., & Jaramillo López, A. M. (2022, January). The Intersection of Workplace and Environmental Exposure on Health in Latinx Farm Working Communities in Rural Inland Southern California. *International Journal of Environmental Research and Public Health*, *19*(19), 12940. doi: 10.3390/ijerph191912940

Cheng, V., Ng, E., Chan, C., & Givoni, B. (2012, January). Outdoor thermal comfort study in a sub-tropical climate: A longitudinal study based in Hong Kong. *International Journal of Biometeorology*, *56*(1), 43–56. doi: 10.1007/s00484-010-0396-z

Chow, W. T. L., Akbar, S. N. A. B. A., Heng, S. L., & Roth, M. (2016, January). Assessment of measured and perceived microclimates within a tropical urban forest. *Urban Forestry & Urban Greening*, *16*, 62–75. doi: 10.1016/j.ufug.2016.01.010

Coffel, E. D., Horton, R. M., & de Sherbinin, A. (2017, December). Temperature and humidity based projections of a rapid rise in global heat stress exposure during the 21st century. *Environmental Research Letters*, *13*(1), 014001. doi: 10.1088/1748-9326/aaa00e

Cooper, E., Grundstein, A., Rosen, A., Miles, J., Ko, J., & Curry, P. (2017, December). An Evaluation of Portable Wet Bulb Globe Temperature Monitor Accuracy. *Journal of Athletic Training*, *52*(12), 1161–1167. doi: 10.4085/1062-6050-52.12.18

Courville, M. D., Wadsworth, G., & Schenker, M. (2016, March). "We Just Have To Continue Working": Farmworker Self-care and Heat-related Illness. *Journal of Agriculture, Food Systems, and Community Development*, *6*(2), 143–164. doi: 10.5304/jafscd.2016.062.014

Dally, M., Butler-Dawson, J., Sorensen, C. J., Van Dyke, M., James, K. A., Krisher, L., ... Newman, L. S. (2020, January). Wet Bulb Globe Temperature and Recorded Occupational Injury Rates among Sugarcane Harvesters in Southwest Guatemala. *International Journal of Environmental Research and Public Health*, *17*(21), 8195. doi: 10.3390/ijerph17218195

Day, E., Fankhauser, S., Kingsmill, N., Costa, H., & Mavrogianni, A. (2019, March). Upholding labour productivity under climate change: An assessment of adaptation options. *Climate Policy*, *19*(3), 367–385. doi: 10.1080/14693062.2018.1517640

de De Lima, C. Z., Buzan, J. R., Moore, F. C., Baldos, U. L. C., Huber, M., & Hertel, T. W. (2021, March). Heat stress on agricultural workers exacerbates crop impacts of climate change. *Environmental Research Letters*, *16*(4), 044020. doi: 10.1088/1748-9326/abeb9f

Diaz, C., Ting, M., Horton, R. M., Singh, D., Rogers, C. D. W., & Coffel, E. D. (2023). Increased extreme humid heat hazard faced by agricultural workers - IOPscience. *Environmental Research Communications*, *5*(11). doi: 10.1088/2515-7620/ad028d

Disciglio, G., Frabboni, L., Tarantino, A., & Stasi, A. (2023, January). Association between Dynamic Agrivoltaic System and Cultivation: Viability, Yields and Qualitative Assessment of Medical Plants. *Sustainability*, *15*(23), 16252. doi: 10.3390/su152316252

Disciglio, G., Stasi, A., Tarantino, A., & Frabboni, L. (2025, January). Microclimate Modification, Evapotranspiration, Growth and Essential Oil Yield of Six Medicinal Plants Cultivated Beneath a Dynamic Agrivoltaic System in Southern Italy. *Plants*, *14*(15), 2428. doi: 10.3390/plants14152428

Dupraz, C., Marrou, H., Talbot, G., Dufour, L., Nogier, A., & Ferard, Y. (2011, October). Combining solar photovoltaic panels and food crops for optimising land use: Towards new agrivoltaic schemes. *Renewable Energy*, *36*(10), 2725–2732. doi: 10.1016/j.renene.2011.03.005

Edgerly, A., Gillespie, G. L., Hittle, B. M., & Bhattacharya, A. (2024). US Farmworkers' Barriers to Preventing Heat-Related Illness: An Integrative Review. *Public Health Challenges*, *3*(3), e222. doi: 10.1002/puh2.222

El Khayat, M., Halwani, D. A., Hneiny, L., Alameddine, I., Haidar, M. A., & Habib, R. R. (2022, February). Impacts of Climate Change and Heat Stress on Farmworkers' Health: A Scoping Review. *Frontiers in Public Health*, *10*. doi: 10.3389/fpubh.2022.782811

Fagnano, M., Fiorentino, N., Visconti, D., Baldi, G. M., Falce, M., Acutis, M., ... Di Blasi, M. (2024, March). Effects of a Photovoltaic Plant on Microclimate and Crops' Growth in a Mediterranean Area. *Agronomy*, *14*(3), 466. doi: 10.3390/agronomy14030466

Fan, Y., & McColl, K. A. (2024, December). Widespread outdoor exposure to uncompensable heat stress with warming. *Communications Earth & Environment*, *5*(1), 1–13. doi: 10.1038/s43247-024-01930-6

Ferguson, D. B. (1988, January). The control of body temperature. In D. B. Ferguson (Ed.), *Physiology for Dental Students* (pp. 309–314). Butterworth-Heinemann. doi: 10.1016/B978-0-7236-0725-0.50028-9

Flouris, A. D., Dinas, P. C., Ioannou, L. G., Nybo, L., Havenith, G., Kenny, G. P., & Kjellstrom, T. (2018, December). Workers' health and productivity under occupational heat strain: A systematic review and meta-analysis. *The Lancet Planetary Health*, *2*(12), 521–531. doi: 10.1016/S2542-5196(18)30237-7

Foster, J., Smallcombe, J. W., Hodder, S., Jay, O., Flouris, A. D., & Havenith, G. (2022, March). Quantifying the impact of heat on human physical work capacity; part II: The observed interaction of air velocity with temperature, humidity, sweat rate, and clothing is not captured by most heat stress indices. *International Journal of Biometeorology*, *66*(3), 507–520. doi: 10.1007/s00484-021-02212-y

Gao, C., Kuklane, K., Östergren, P.-O., & Kjellstrom, T. (2018, March). Occupational heat stress assessment and protective strategies in the context of climate change. *International Journal of Biometeorology*, *62*(3), 359–371. doi: 10.1007/s00484-017-1352-y

Gillett, N. P., Kirchmeier-Young, M., Ribes, A., Shiogama, H., Hegerl, G. C., Knutti, R., ... Ziehn, T. (2021, March). Constraining human contributions to observed warming since the pre-industrial period. *Nature Climate Change*, *11*(3), 207–212. doi: 10.1038/s41558-020-00965-9

Gilman, P., Dobos, A., DiOrio, N., Freeman, J., Janzou, S., & Ryberg, D. (2018). *SAM Photovoltaic Model Technical Reference Update.* National Renewable Energy Labratory.

Giri, N. C., & Mohanty, R. C. (2022, October). Agrivoltaic system: Experimen-

tal analysis for enhancing land productivity and revenue of farmers. *Energy for Sustainable Development*, *70*, 54–61. doi: 10.1016/j.esd.2022.07.003

Gonocruz, R. A., Nakamura, R., Yoshino, K., Homma, M., Doi, T., Yoshida, Y., & Tani, A. (2021, July). Analysis of the Rice Yield under an Agrivoltaic System: A Case Study in Japan. *Environments*, *8*(7), 65. doi: 10.3390/environments8070065

Hackenberg, A., Kappertz, L., Rapol, S., Solovievskyi, V., & Büskens, C. (2023). Optimal photovoltaic plant dimensioning using consumption data. , *23*(1). doi: 10.1002/pamm.202200250

Haldane, J. S. (1905, October). The Influence of High Air Temperatures No. I. *Epidemiology & Infection*, *5*(4), 494–513. doi: 10.1017/S0022172400006811

Hanna, E., & Tait, P. (2015). Limitations to Thermoregulation and Acclimatization Challenge Human Adaptation to Global Warming. *Climate Chnange and Human Health*, *12*(7), 8034–8074. doi: 10.3390/ijerph120708034

Havenith, G., & Fiala, D. (2015). Thermal Indices and Thermophysiological Modeling for Heat Stress. In *Comprehensive Physiology* (pp. 255–302). John Wiley & Sons, Ltd. doi: 10.1002/cphy.c140051

Helou, N. E., Tafflet, M., Berthelot, G., Tolaini, J., Marc, A., Guillaume, M., ... Toussaint, J.-F. (2012, May). Impact of Environmental Parameters on Marathon Running Performance. *PLOS ONE*, *7*(5), e37407. doi: 10.1371/journal.pone.0037407

Honningdalsnes, E., Marstein, E., Lindholm, D., Bonesmo, H., & Riise, H. (2025, September). Wind sheltering in vertical agrivoltaics can increase crop yields: A modeling study for Northern Europe. *Energy Nexus*, *19*, 100516. doi: 10.1016/j.nexus.2025.100516

Huang, L., & Zhai, Z. J. (2020, October). Critical review and quantitative evaluation of indoor thermal comfort indices and models incorporating solar radiation effects. *Energy and Buildings*, *224*, 110204. doi: 10.1016/j.enbuild.2020.110204

Hudelson, T., & Lieth, J. H. (2021, June). Crop production in partial shade of solar photovoltaic panels on trackers. *AIP Conference Proceedings*, *2361*(1), 080001. doi: 10.1063/5.0055174

Hwang, R.-L., & Lin, T.-P. (2007, December). Thermal Comfort Requirements for Occupants of Semi-Outdoor and Outdoor Environments in Hot-Humid Regions. *Architectural Science Review*, *50*(4), 357–364. doi: 10.3763/asre.2007.5043

Irani, T., Pierre, B. F., & Nesbit, T. S. (2021, January). Agricultural Stakeholders' Perceptions of Occupational Health and Safety in the Southeastern U.S. Coastal States. *International Journal of Environmental Research and Public Health*, *18*(12), 6605. doi: 10.3390/ijerph18126605

Jacobs, C., Singh, T., Gorti, G., Iftikhar, U., Saeed, S., Syed, A., ... Siderius, C. (2019, July). Patterns of outdoor exposure to heat in three South Asian cities. *Science of The Total Environment*, *674*, 264–278. doi: 10.1016/j.scitotenv.2019.04.087

Johansson, E., & Emmanuel, R. (2006, November). The influence of urban design on outdoor thermal comfort in the hot, humid city of Colombo, Sri Lanka. *International Journal of Biometeorology*, *51*(2), 119–133. doi: 10.1007/s00484-006-0047-6

Juillion, P., Tranchant, C., Nadi, K., Noel, J., Valle, B., Chopard, J., ... Fumey, D. (2024). Effects of Dynamic Agrivoltaics on Containerized Raspberry Plants: Results of the First Season. *AgriVoltaics Conference Proceedings*, *3*. doi: 10.52825/agripv.v3i.1405

Kang, S., & Eltahir, E. A. B. (2018, July). North China Plain threatened by deadly heatwaves due to climate change and irrigation. *Nature Communications*, *9*(1), 2894. doi: 10.1038/s41467-018-05252-y

Kantor, N., Chen, L., & Gal, C. (2018, February). Human-biometeorological significance of shading in urban public spaces—Summertime measurements in Pécs, Hungary. *Landscape and Urban Planning*, *170*, 241–255. doi: 10.1016/j.landurbplan.2017.09.030

Katsikogiannis, O. A., Ziar, H., & Isabella, O. (2022, March). Integration of bifacial photovoltaics in agrivoltaic systems: A synergistic design approach. *Applied Energy*, *309*, 118475. doi: 10.1016/j.apenergy.2021.118475

Kavga, A., Trypanagnostopoulos, G., Zervoudakis, G., & Tripanagnostopoulos, Y. (2018, January). Growth and Physiological Characteristics of Lettuce (Lactuca sativa L.) and Rocket (Eruca sativa Mill.) Plants Cultivated under Photovoltaic Panels. *Notulae Botanicae Horti Agrobotanici Cluj-Napoca*, *46*(1), 206–212. doi: 10.15835/nbha46110846

Kearney, G. D., Hu, H., Xu, X., Hall, M. B., & Balanay, J. A. G. (2016, January). Estimating the Prevalence of Heat-Related Symptoms and Sun Safety–Related Behavior among Latino Farmworkers in Eastern North Carolina. *Journal of Agromedicine*, *21*(1), 15–23. doi: 10.1080/1059924X.2015.1106377

Kim, S., & Kim, S. (2023, August). Design of an Agrivoltaic System with Building Integrated Photovoltaics. *Agronomy*, *13*(8), 2140. doi: 10.3390/agronomy13082140

Kjellstrom, T., Briggs, D., Freyberg, C., Lemke, B., Otto, M., & Hyatt, O. (2016, March). Heat, Human Performance, and Occupational Health: A Key Issue for the Assessment of Global Climate Change Impacts. *Annual Review of Public Health*, *37*(Volume 37, 2016), 97–112. doi: 10.1146/annurev-publhealth-032315-021740

Kjellstrom, T., Maitre, N., Saget, C., Otto, M., & Karimova, T. (2019). *Working on a Warmer Planet: The Impact of Heat Stress on Labour Productivity and Decent Work* (Tech. Rep.). Geneva, Switzerland: International Labour Office.

Koop, L. K., & Tadi, P. (2024). Physiology, Heat Loss. In *StatPearls*. Treasure Island (FL): StatPearls Publishing.

Koppe, C., Kovats, S., Jendritzky, G., & Menne, B. (2004). *Heat-waves: Risks and responses.* World Health Organisation. Regional Office for Europe.

Kottek, M., Grieser, J., Beck, C., Rudolf, B., & Rubel, F. (2006). World Map of the Köppen-Geiger Climate Classification Updated. *Meteorologische Zeitschrift*, *15*(3), 259–263. doi: 10.1127/0941-2948/2006/0130

Langer, C. E., Mitchell, D. C., Armitage, T. L., Moyce, S. C., Tancredi, D. J., Castro, J., ... Schenker, M. B. (2021, June). Are Cal/OSHA Regulations Protecting Farmworkers in California From Heat-Related Illness? *Journal of Occupational and Environmental Medicine*, *63*(6), 532. doi: 10.1097/JOM.0000000000002189

Lepley, K., Fields, H., Choi, C. S., Hickey, T., Towner, B., Staie, B., ... Macknick, J. (2025, January). Comprehensive Evaluation of Agrivoltaics Research: Breadth, Depth, and Insights for Future Research. *Energies*, *18*(17), 4776. doi: 10.3390/en18174776

Lesk, C., Anderson, W., Rigden, A., Coast, O., Jägermeyr, J., McDermid, S., ... Konar, M. (2022, December). Compound heat and moisture extreme impacts on global crop yields under climate change. *Nature Reviews Earth & Environment*, *3*(12), 872–889. doi: 10.1038/s43017-022-00368-8

Li, H., & Sun, S. (2024). Exploration of the European agrivoltaics landscape in the context of global climate change. *E3S Web of Conferences*, *520*, 02013. doi: 10.1051/e3sconf/202452002013

Liljegren, J. C., Carhart, R. A., Lawday, P., Tschopp, S., & Sharp, R. (2008, September). Modeling the Wet Bulb Globe Temperature Using Standard Meteorological Measurements. *Journal of Occupational and Environmental Hygiene*, *5*(10), 645–655. doi: 10.1080/15459620802310770

Liu, Z., Li, J., & Xi, T. (2023, December). A Review of Thermal Comfort Evalua-

tion and Improvement in Urban Outdoor Spaces. *Buildings*, *13*(12), 3050. doi: 10.3390/buildings13123050

Lopez, G., Chopard, S., Persello, S., Juilion, P., Lesniak, V., Vercambre, G., ... Fumey, D. (2023). Agrivoltaic systems: An innovative technique to protect fruit trees from climate change | International Society for Horticultural Science. *Acta Horticulturae*, 173–186. doi: 10.17660/ActaHortic.2023.1366.20

Lopez, G., Pasquali, A., Hitte, V., Lesniak, V., Bregeon, M., Persello, S., ... Fumey, D. (2024). Sun Protection for Fruit: Dynamic Agrivoltaics Reduces Apple Temperature and Sunburn Damage. *AgriVoltaics Conference Proceedings*, *3*. doi: 10.52825/agripv.v3i.1371

Ludzuweit, A., Paterson, J., Wydra, K., Pump, C., Müller, K., & Miller, Y. (2025, April). Enhancing ecosystem services and biodiversity in agrivoltaics through habitat-enhancing strategies. *Renewable and Sustainable Energy Reviews*, *212*, 115380. doi: 10.1016/j.rser.2025.115380

Lüthi, S., Fairless, C., Fischer, E., & et al. (2023). Rapid increase in the risk of heat-related mortality. *Nature Communications*, *14*. doi: 10.1038/s41467-023-40599-x

Magarelli, A., Mazzeo, A., & Ferrara, G. (2024, April). Fruit Crop Species with Agrivoltaic Systems: A Critical Review. *Agronomy*, *14*(4), 722. doi: 10.3390/agronomy14040722

Marrou, H., Guilioni, L., Dufour, L., Dupraz, C., & Wery, J. (2013, August). Microclimate under agrivoltaic systems: Is crop growth rate affected in the partial shade of solar panels? *Agricultural and Forest Meteorology*, *177*, 117–132. doi: 10.1016/j.agrformet.2013.04.012

Marrou, H., Wery, J., Dufour, L., & Dupraz, C. (2013, January). Productivity and radiation use efficiency of lettuces grown in the partial shade of photovoltaic panels. *European Journal of Agronomy*, *44*, 54–66. doi: 10.1016/j.eja.2012.08.003

Middel, A., AlKhaled, S., Schneider, F. A., Hagen, B., & Coseo, P. (2021, October). 50 Grades of Shade.
doi: 10.1175/BAMS-D-20-0193.1

Middel, A., & Krayenhoff, E. S. (2019, October). Micrometeorological determinants of pedestrian thermal exposure during record-breaking heat in Tempe, Arizona: Introducing the MaRTy observational platform. *Science of The Total Environment*, *687*, 137–151. doi: 10.1016/j.scitotenv.2019.06.085

Minard, D., Belding, H. S., & Kingston, J. R. (1957, December). PREVENTION OF HEAT CASUALTIES. *Journal of the American Medical Association*, *165*(14), 1813–1818. doi: 10.1001/jama.1957.02980320043010

Mishra, V., Ambika, A. K., Asoka, A., Aadhar, S., Buzan, J., Kumar, R., & Huber, M. (2020, November). Moist heat stress extremes in India enhanced by irrigation. *Nature Geoscience*, *13*(11), 722–728. doi: 10.1038/s41561-020-00650-8

Mitchell, D., Heaviside, C., Vardoulakis, S., Huntingford, C., Masato, G., Guillod, B., ... Allen, M. (2016). Attributing human mortality during extreme heat waves to anthropogenic climate change - IOPscience. , *11*. doi: 10.1088/1748-9326/11/7/074006

Moda, H. M., Filho, W. L., & Minhas, A. (2019, September). Impacts of Climate Change on Outdoor Workers and Their Safety: Some Research Priorities. *International Journal of Environmental Research and Public Health*, *16*(18), 3458. doi: 10.3390/ijerph16183458

Mohammedi, S., Dragonetti, G., Admane, N., & Fouial, A. (2023, December). The Impact of Agrivoltaic Systems on Tomato Crop: A Case Study in Southern Italy. *Processes*, *11*(12), 3370. doi: 10.3390/pr11123370

Mohseni, S., & Brent, A. (2024). Operational Dispatch Optimization of an Agrivoltaic System. *AgriVoltaics Conference Proceedings*, *3*. doi: 10.52825/agripv.v3i.1348

Moon, H.-W., & Ku, K.-M. (2022, January). Impact of an Agriphotovoltaic System on Metabolites and the Sensorial Quality of Cabbage (Brassica oleracea var. capitata) and Its High-Temperature-Extracted Juice. *Foods*, *11*(4), 498. doi: 10.3390/foods11040498

Mora, C., Dousset, B., Caldwell, I. R., Powell, F. E., Geronimo, R. C., Bielecki, C. R., ... Trauernicht, C. (2017, July). Global risk of deadly heat. *Nature Climate Change*, *7*(7), 501–506. doi: 10.1038/nclimate3322

Morabito, M., Messeri, A., Crisci, A., Bao, J., Ma, R., Orlandini, S., ... Kjellstrom, T. (2020, January). Heat-related productivity loss: Benefits derived by working in the shade or work-time shifting. *International Journal of Productivity and Performance Management*, *70*(3), 507–525. doi: 10.1108/IJPPM-10-2019-0500

Morera, M. C., Gusto, C., Monaghan, P. F., Tovar-Aguilar, J. A., & Roka, F. M. (2020, September). "We Force Ourselves": Productivity, Workplace Culture, and HRI Prevention in Florida's Citrus Groves. *Safety*, *6*(3), 41. doi: 10.3390/safety6030041

Moyce, S., Mitchell, D., Armitage, T., Tancredi, D., Joseph, J., & Schenker, M. (2017, June). Heat strain, volume depletion and kidney function in California agricultural workers. *Occupational and Environmental Medicine*, *74*(6), 402–409. doi: 10.1136/oemed-2016-103848

Mupambi, G., Sandler, H., & Jeranyama, P. (2022, March). Installation of an agrivoltaic system influences microclimatic conditions and leaf gas exchange in cranberry. *Acta Horticulturae*(1337), 117–124. doi: 10.17660/ActaHortic.2022.1337.16

Nelson, G. C., Vanos, J., Havenith, G., Jay, O., Ebi, K. L., & Hijmans, R. J. (2024). Global reductions in manual agricultural work capacity due to climate change. *Global Change Biology*, *30*(1), e17142. doi: 10.1111/gcb.17142

Nielsen, B., Kassow, K., & Aschengreen, F. E. (1988, January). Heat balance during exercise in the sun. *European Journal of Applied Physiology and Occupational Physiology*, *58*(1), 189–196. doi: 10.1007/BF00636625

NIOSH. (2016). *Criteria for a recommended standard: Occupational exposure to heat and hot environments* (Tech. Rep. No. 106). Cincinnati, OH: National Institute for Occupational Safety and Health.

Osilla, E. V., Marsidi, J. L., Shumway, K. R., & Sharma, S. (2024). Physiology, Temperature Regulation. In *StatPearls.* Treasure Island (FL): StatPearls Publishing.

Otani, H., Kaya, M., Tamaki, A., Watson, P., & Maughan, R. J. (2016, April). Effects of solar radiation on endurance exercise capacity in a hot environment. *European Journal of Applied Physiology*, *116*(4), 769–779. doi: 10.1007/s00421-016-3335-9

Othman, N. F., Ya'acob, M. E., Lu, L., Jamaluddin, A. H., Mat Su, A. S., Hizam, H., ... Jaafar, J. N. (2023, April). Advancement in Agriculture Approaches with Agrivoltaics Natural Cooling in Large Scale Solar PV Farms. *Agriculture*, *13*(4), 854. doi: 10.3390/agriculture13040854

Palmer, T. N. (2013, April). Climate extremes and the role of dynamics. *Proceedings of the National Academy of Sciences*, *110*(14), 5281–5282. doi: 10.1073/pnas.1303295110

Parsons, K. (2006). Heat Stress Standard ISO 7243 and its Global Application. doi: 10.2486/indhealth.44.368

Patel, T., Mullen, S. P., & Santee, W. R. (2013, August). Comparison of Methods for Estimating Wet-Bulb Globe Temperature Index From Standard Meteorological Measurements. *Military Medicine*, *178*(8), 926–933. doi: 10.7205/MILMED-D-13-00117

Petropoulos, Z. E., Ramirez-Rubio, O., Scammell, M. K., Laws, R. L., Lopez-Pilarte, D., Amador, J. J., ... Brooks, D. R. (2021, January). Climate Trends at a

Hotspot of Chronic Kidney Disease of Unknown Causes in Nicaragua, 1973–2014. *International Journal of Environmental Research and Public Health*, *18*(10), 5418. doi: 10.3390/ijerph18105418

Piil, J. F., Christiansen, L., Morris, N. B., Mikkelsen, C. J., Ioannou, L. G., Flouris, A. D., ... Nybo, L. (2020, May). Direct exposure of the head to solar heat radiation impairs motor-cognitive performance. *Scientific Reports*, *10*(1), 7812. doi: 10.1038/s41598-020-64768-w

Platt, M., & Vicario, S. (2013). Heat Illness. In *Rosen's Emergency Medicine - Concepts and Clinical Practice* (7th ed., pp. 1882–1889). Philadelphia, PA: Elsevier.

Poppick, A., & McKinnon, K. A. (2020, December). Observation-Based Simulations of Humidity and Temperature Using Quantile Regression. doi: 10.1175/JCLI-D-20-0403.1

Powis, C. M., Byrne, D., Zobel, Z., Gassert, K. N., Lute, A. C., & Schwalm, C. R. (2023, September). Observational and model evidence together support widespread exposure to noncompensable heat under continued global warming. *Science Advances*, *9*(36), eadg9297. doi: 10.1126/sciadv.adg9297

Proutsos, N., Alexandris, S., Liakatas, A., Nastos, P., & Tsiros, I. X. (2022, May). PAR and UVA composition of global solar radiation at a high altitude Mediterranean forest site. *Atmospheric Research*, *269*, 106039. doi: 10.1016/j.atmosres.2022.106039

Ravanelli, N. M., Hodder, S. G., Havenith, G., & Jay, O. (2015, February). Heart Rate and Body Temperature Responses to Extreme Heat and Humidity With and Without Electric Fans. *JAMA*, *313*(7), 724–725. doi: 10.1001/jama.2015.153

Ravishankar, E., Esh, S., Rozenstein, O., Vitoshkin, H., Kribus, A., Mittelman, G., ... Hernandez, R. (2023). Improved Land Use Efficiency Through Spectral Beam Splitting in Agrivoltaic Farms. *AgriVoltaics Conference Proceedings*, *2*. doi: 10.52825/agripv.v2i.997

Raymond, C., Matthews, T., & Horton, R. M. (2020, May). The emergence of heat and humidity too severe for human tolerance. *Science Advances*, *6*(19), eaaw1838. doi: 10.1126/sciadv.aaw1838

Reda, I., & Andreas, A. (2008). *Solar Position Algorithm for Solar Radiation Applications* (Tech. Rep.). Golden, Colorado: National Renewable Energy Labratory.

Riaz, M., Imran, H., Younas, R., & Butt, N. (2021, December). The optimization of vertical bifacial photovoltaic farms for efficient agrivoltaic systems. *Solar Energy*, *230*, 1004–1012. doi: 10.1016/j.solener.2021.10.051

Rogers, C. D. W., Ting, M., Li, C., Kornhuber, K., Coffel, E. D., Horton, R. M., ... Singh, D. (2021). Recent Increases in Exposure to Extreme Humid-Heat Events Disproportionately Affect Populated Regions. *Geophysical Research Letters*. doi: 10.1029/2021GL094183

Rouini, N., Salazar, A., Murphy, P., Lepley, K., & Barron-Gafford, G. A. (2025, October). High-shade dryland agrivoltaic conditions enhanced carbon uptake and water-use efficiency in zucchini (Cucurbita pepo). *Frontiers in Sustainable Food Systems*, *9*. doi: 10.3389/fsufs.2025.1686773

Russo, S., Sillmann, J., & Sterl, A. (2017). Humid heat waves at different warming levels. *Scientific Reports*, *7*. doi: 10.1038/s41598-017-07536-7

Sarr, A., Soro, Y. M., Tossa, A. K., & Diop, L. (2023, March). Agrivoltaic, a Synergistic Co-Location of Agricultural and Energy Production in Perpetual Mutation: A Comprehensive Review. *Processes*, *11*(3), 948. doi: 10.3390/pr11030948

Sawka, M. N., Leon, L. R., Montain, S. J., & Sonna, L. A. (2011, October). Integrated Physiological Mechanisms of Exercise Performance, Adaptation, and Maladaptation to Heat Stress. In Y. S. Prakash (Ed.), *Comprehensive Physiol-*

ogy (1st ed., pp. 1883–1928). Wiley. doi: 10.1002/cphy.c100082

Schauberger, B., Archontoulis, S., Arneth, A., Balkovic, J., Ciais, P., Deryng, D., ... Frieler, K. (2017, January). Consistent negative response of US crops to high temperatures in observations and crop models. *Nature Communications*, *8*(1), 13931. doi: 10.1038/ncomms13931

Sekiyama, T., & Nagashima, A. (2019, June). Solar Sharing for Both Food and Clean Energy Production: Performance of Agrivoltaic Systems for Corn, A Typical Shade-Intolerant Crop. *Environments*, *6*(6), 65. doi: 10.3390/environments6060065

Sherwood, S. C. (2018). How Important Is Humidity in Heat Stress? *Journal of Geophysical Research: Atmospheres*, *123*(21), 11,808–11,810. doi: 10.1029/2018JD028969

Sherwood, S. C., & Huber, M. (2010, May). An adaptability limit to climate change due to heat stress. doi: 10.1073/pnas.0913352107

Si, Y., Wang, Y., Cao, Y., & Si, D. (2024, January). Comprehensive Utilisation and Performance Optimisation of Agro-electricity and Agro-photovoltaic Complementary Systems in Agricultural Production. *Transactions on Economics, Business and Management Research*, *4*, 38–43. doi: 10.62051/73tdky89

Simpson, C., Hosking, J. S., Mitchell, D., Betts, R. A., & Shuckburgh, E. (2021, November). Regional disparities and seasonal differences in climate risk to rice labour. *Environmental Research Letters*, *16*(12), 124004. doi: 10.1088/1748-9326/ac3288

Spector, J. T., Bonauto, D. K., Sheppard, L., Busch-Isaksen, T., Calkins, M., Adams, D., ... Fenske, R. A. (2016, October). A Case-Crossover Study of Heat Exposure and Injury Risk in Outdoor Agricultural Workers. *PLOS ONE*, *11*(10), e0164498. doi: 10.1371/journal.pone.0164498

Spector, J. T., Krenz, J., & Blank, K. N. (2015). Risk factors for heat-related illness in Washington crop workers. *Journal of agromedicine*, *20*(3), 349–359.

Thompson, E. P., Bombelli, E. L., Shubham, S., Watson, H., Everard, A., D'Ardes, V., ... Bombelli, P. (2020). Tinted Semi-Transparent Solar Panels Allow Concurrent Production of Crops and Electricity on the Same Cropland. *Advanced Energy Materials*, *10*(35), 2001189. doi: 10.1002/aenm.202001189

Thum, C. H., Okada, K., Yamasaki, Y., & Kato, Y. (2025, May). Impacts of agrivoltaic systems on microclimate, grain yield, and quality of lowland rice under a temperate climate. *Field Crops Research*, *326*, 109877. doi: 10.1016/j.fcr.2025.109877

Tigchelaar, M., Battisti, D. S., & Spector, J. T. (2020, August). Work adaptations insufficient to address growing heat risk for U.S. agricultural workers. *Environmental Research Letters*, *15*(9), 094035. doi: 10.1088/1748-9326/ab86f4

Ting, M., Lesk, C., Liu, C., Li, C., Horton, R. M., Coffel, E. D., ... Singh, D. (2023, January). Contrasting impacts of dry versus humid heat on US corn and soybean yields. *Scientific Reports*, *13*(1), 710. doi: 10.1038/s41598-023-27931-7

Trommsdorff, M., Kang, J., Reise, C., Schindele, S., Bopp, G., Ehmann, A., ... Oberfell, T. (2021, April). Combining food and energy production: Design of an agrivoltaic system applied in arable and vegetable farming in Germany. *Renewable and Sustainable Energy Reviews*, *140*, 110694. doi: 10.1016/j.rser.2020.110694

Troy, T. J., Kipgen, C., & Pal, I. (2015, May). The impact of climate extremes and irrigation on US crop yields. *Environmental Research Letters*, *10*(5), 054013. doi: 10.1088/1748-9326/10/5/054013

Valle, B., Simonneau, T., Sourd, F., Pechier, P., Hamard, P., Frisson, T., ... Christophe, A. (2017, November). Increasing the total productivity of a land by combining mobile photovoltaic panels and food crops. *Applied Energy*, *206*, 1495–1507. doi: 10.1016/j.apenergy.2017.09.113

Vecellio, D. J., Wolf, S. T., Cottle, R. M., & Kenney, W. L. (2022, February). Evaluating the 35°C wet-bulb temperature adaptability threshold for young, healthy subjects (PSU HEAT Project). *Journal of Applied Physiology*, *132*(2), 340–345. doi: 10.1152/japplphysiol.00738.2021

Weselek, A., Bauerle, A., Hartung, J., Zikeli, S., Lewandowski, I., & Högy, P. (2021, August). Agrivoltaic system impacts on microclimate and yield of different crops within an organic crop rotation in a temperate climate. *Agronomy for Sustainable Development*, *41*(5), 59. doi: 10.1007/s13593-021-00714-y

Weselek, A., Ehmann, A., Zikeli, S., Lewandowski, I., Schindele, S., & Högy, P. (2019, June). Agrophotovoltaic systems: Applications, challenges, and opportunities. A review. *Agronomy for Sustainable Development*, *39*(4), 35. doi: 10.1007/s13593-019-0581-3

Willett, K. M., Gillett, N. P., Jones, P. D., & Thorne, P. W. (2007, October). Attribution of observed surface humidity changes to human influence. *Nature*, *449*(7163), 710–712. doi: 10.1038/nature06207

Willett, K. M., & Sherwood, S. (2012). Exceedance of heat index thresholds for 15 regions under a warming climate using the wet-bulb globe temperature. *International Journal of Climatology*, *32*(2), 161–177. doi: 10.1002/joc.2257

Wyndham, C. H., & Atkins, A. R. (1968, March). A physiological scheme and mathematical model of temperature regulation in man. *Pflügers Archiv*, *303*(1), 14–30. doi: 10.1007/BF00586824

Zastrow, & Goetzberger. (1982). On the Coexistence of Solar-Energy Conversion and Plant Cultivation. *International Journal of Solar Energy*, *1*(1), 55–69. doi: 10.1080/01425918208909875

Zhang, F., Li, M., Zhang, W., Liu, W., Ali Abaker Omer, A., Zhang, Z., ... Zhang, X. (2023, October). Large-scale and cost-efficient agrivoltaics system by spectral separation. *iScience*, *26*(11), 108129. doi: 10.1016/j.isci.2023.108129

Zhang, L., Wei, D., Hou, Y., Du, J., Liu, Z., Zhang, G., & Shi, L. (2020, January). Outdoor Thermal Comfort of Urban Park—A Case Study. *Sustainability*, *12*(5), 1961. doi: 10.3390/su12051961

Zheng, J., Meng, S., Zhang, X., Zhao, H., Ning, X., Chen, F., ... Liu, W. (2021, July). Increasing the comprehensive economic benefits of farmland with Even-lighting Agrivoltaic Systems. *PLOS ONE*, *16*(7), e0254482. doi: 10.1371/journal.pone.0254482

1236 # Supplementary Material

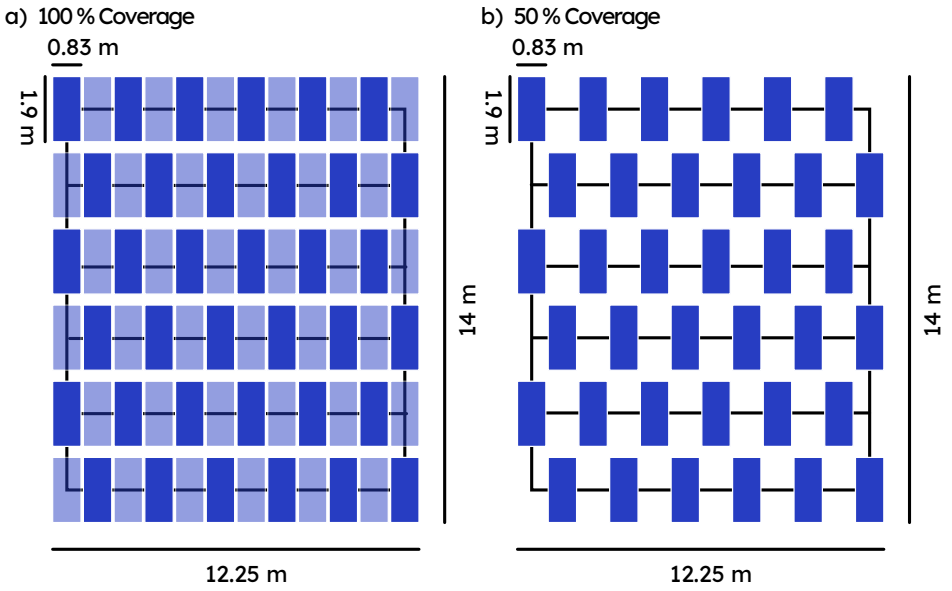

Figure S 1: Birds eye view of the overhead agrivoltaic treatments illustrating a) 100% panel coverage, and b) 50% panel coverage

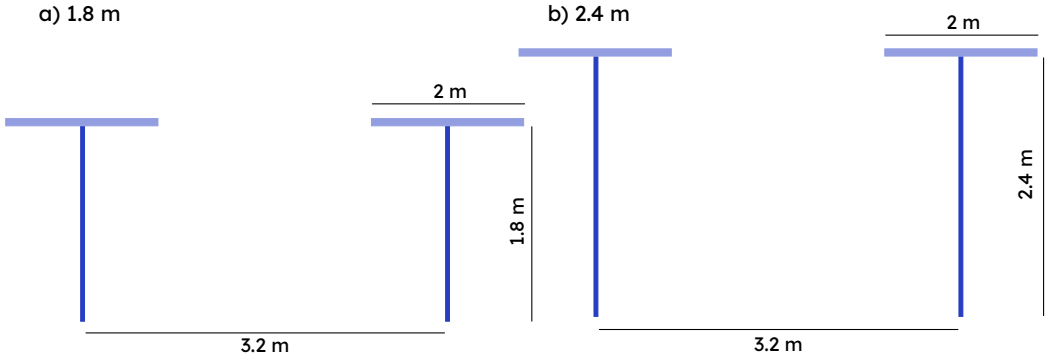

Figure S 2: Side view of the interspaced agrivoltaic treatments illustrating a) 1.8 m, and 2) 2.4 m.

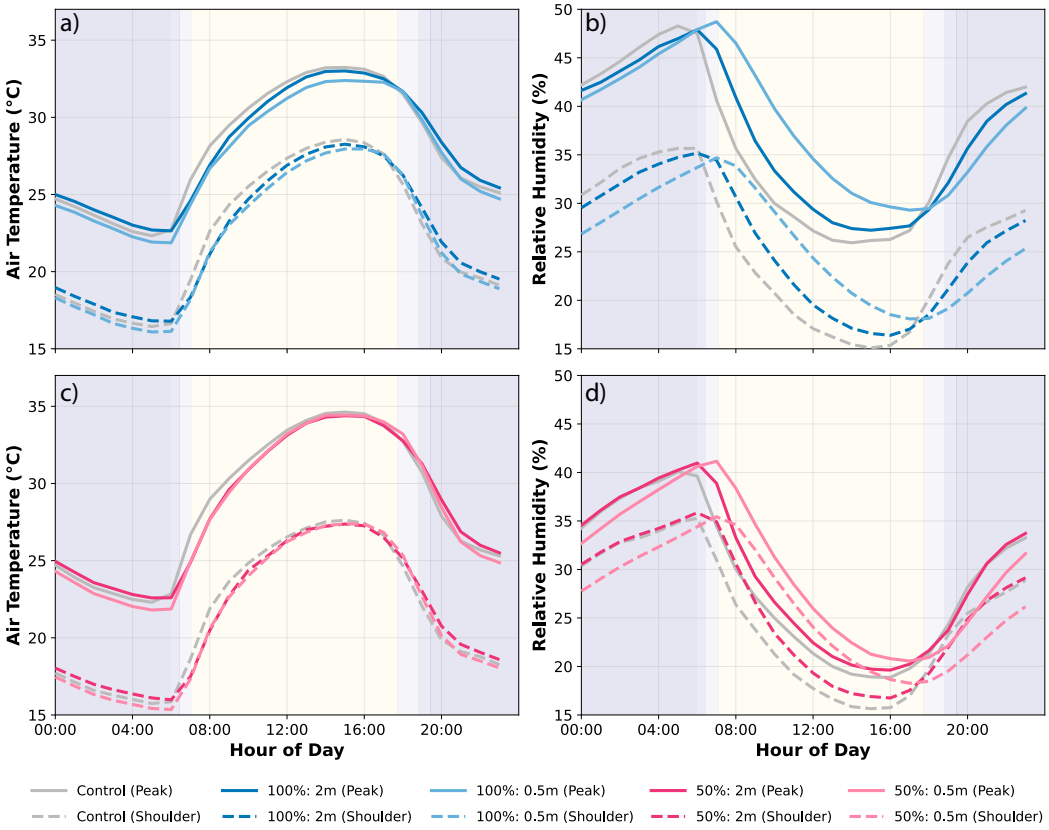

Figure S 3: Diurnal patterns of air temperature and relative humidity at two measurement heights (2 m and 0.5 m) under 100% panel coverage (top row) and 50% panel coverage (bottom row) compared to control conditions. Measurements at 2 m (darker colored line) are used for primary analysis as they match the height of the control sensors, while 0.5 m measurements (lighter colored lines) illustrate vertical microclimate gradients. Solid lines represent peak season (June-August) and dashed lines represent shoulder season (April-May, September-October). Under 100% panel coverage, air temperature at 0.5 m remains cooler for longer compared to 2 m height during daytime hours. Under 50% panel coverage, air temperature at both heights follow similar daytime patterns. In both 100% and 50% panel coverage, relative humidity is substantially higher during the day at 0.5 m compared to 2 m.

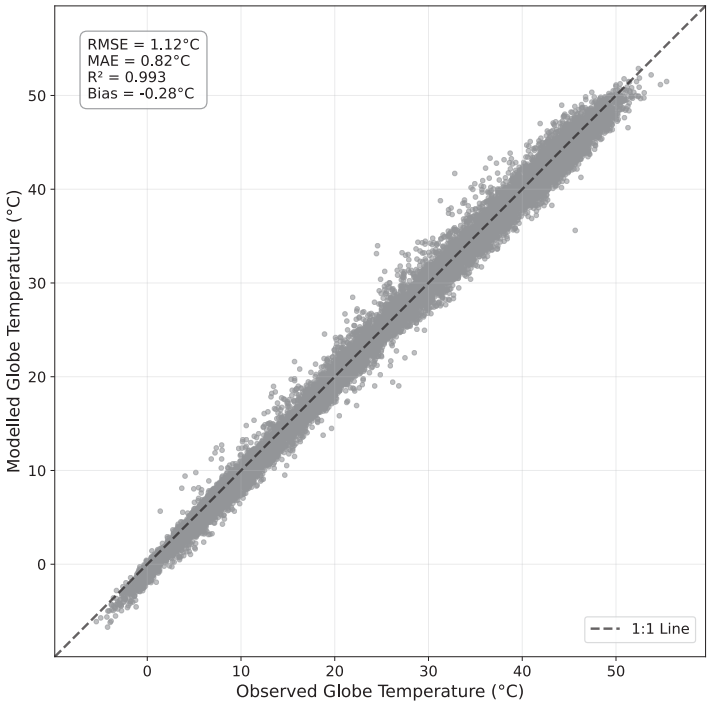

Figure S 4: Comparison of modeled versus observed globe temperatures for the control condition at the overhead agrivoltaic site. The dashed line represents the 1:1 relationship. Statistical metrics show strong model performance with $R^2 = 0.993$, RMSE = 1.12°C, and a small negative bias of -0.28°C.

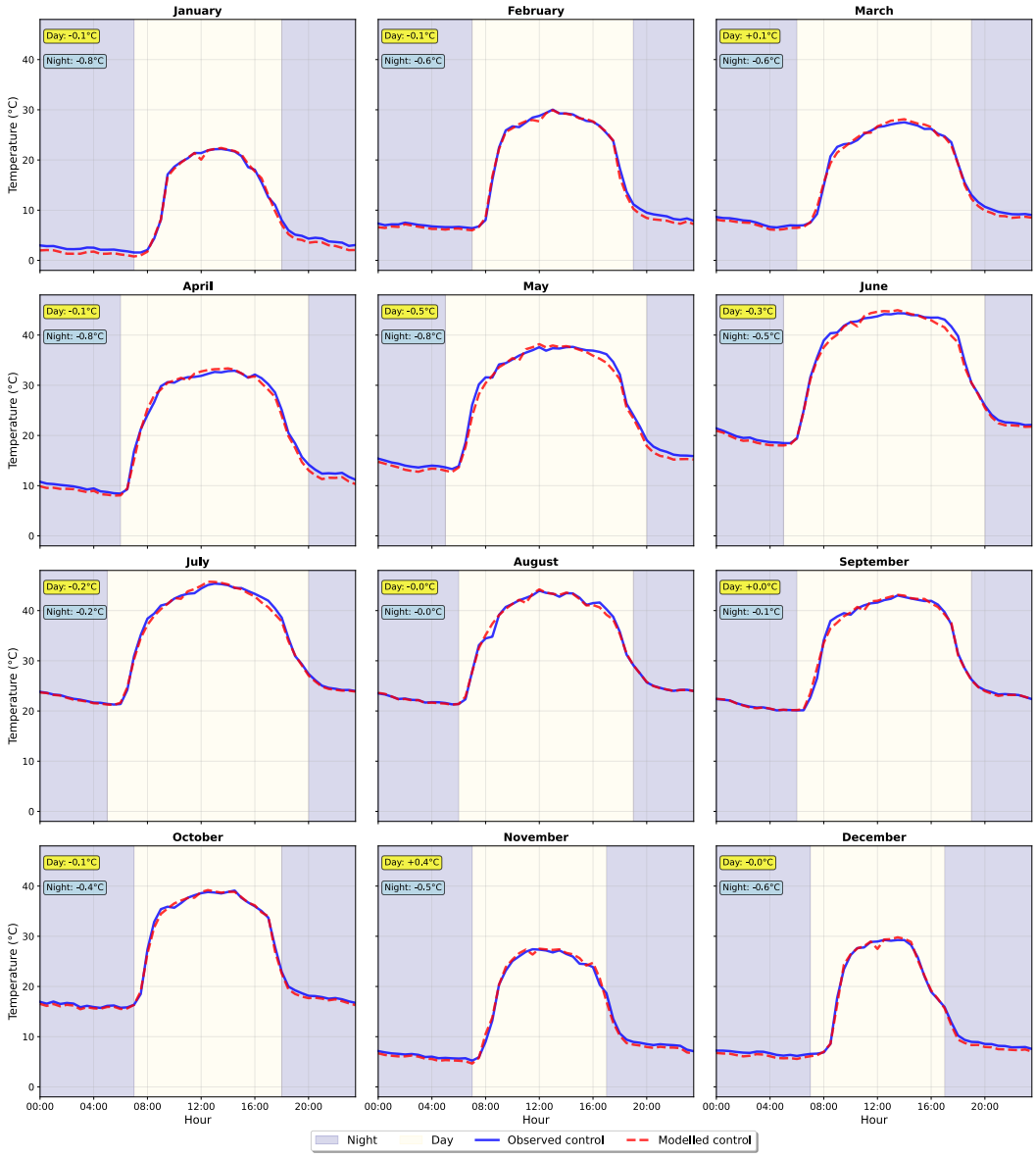

Figure S 5: Monthly diurnal patterns of globe temperatures in control condition at the overhead agrivoltaic site, comparing modeled (red dashed line) and observed (blue solid line) values. Yellow shading indicates daytime hours while blue shading indicated nighttime hours. Bias values shown represent the mean difference between modeled and observed temperatures during day and night periods.

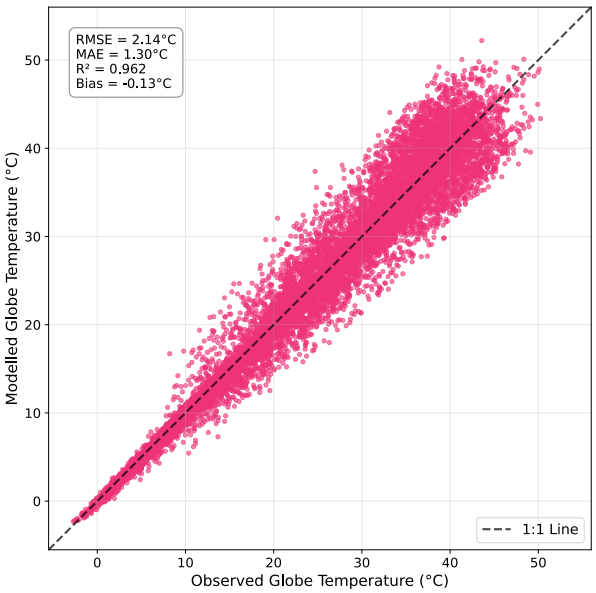

Figure S 6: Comparison of modeled versus observed globe temperatures for the 50% panel cover treatment at the overhead agrivoltaic site. The dashed line represents the 1:1 relationship. Statistical metrics show strong model performance with $R^2 = 0.962$, RMSE = 2.16°C, and a small bias of 0.18°C.

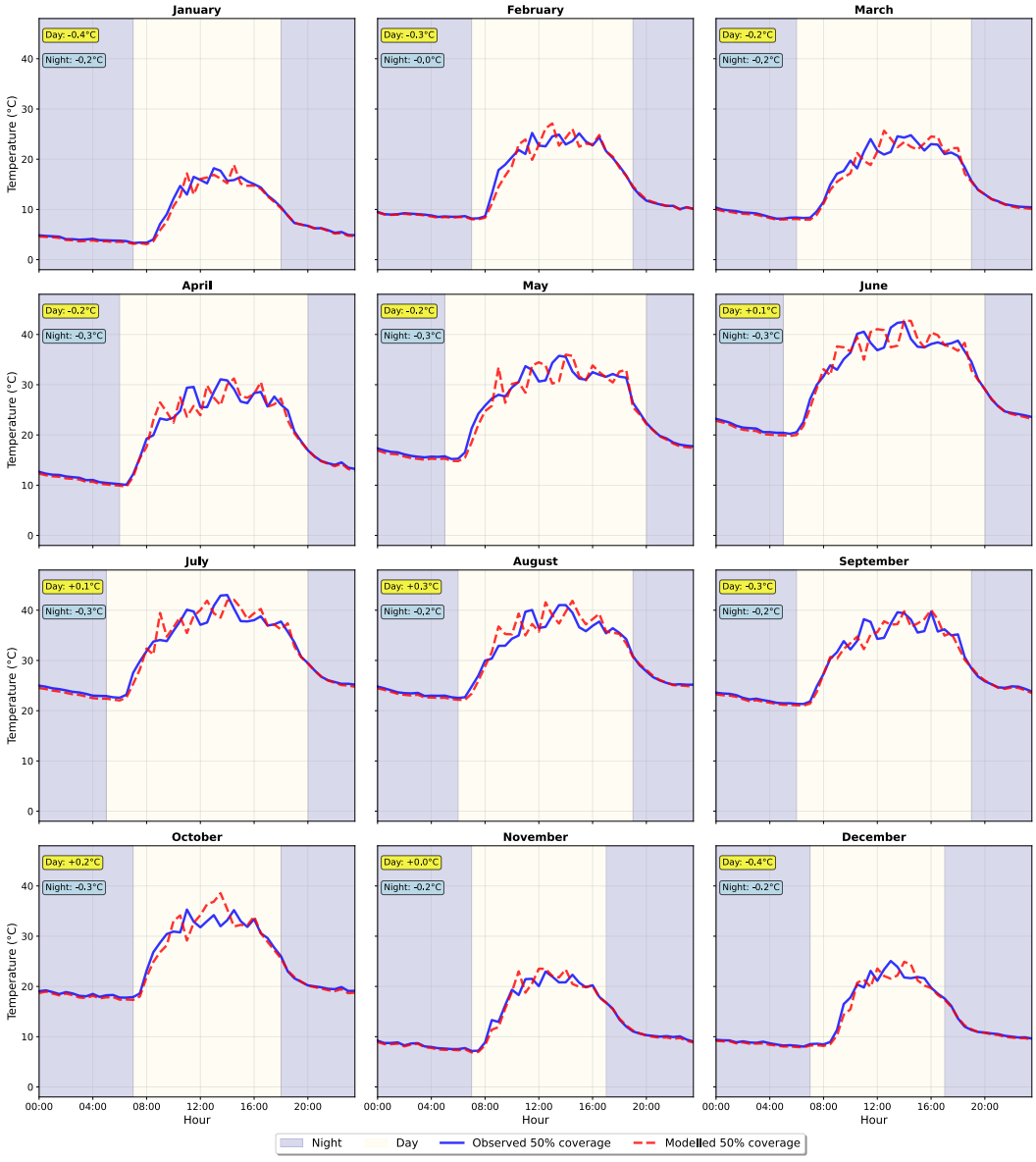

Figure S 7: Monthly diurnal patterns of globe temperatures comparing modeled (red dashed line) and observed (blue solid line) values for the 50% panel coverage overhead agrivoltaic treatment. Yellow shading indicates daytime hours while blue shading indicates nighttime hours. Bias values shown represent the difference between modeled and observed temperatures during day and night periods.

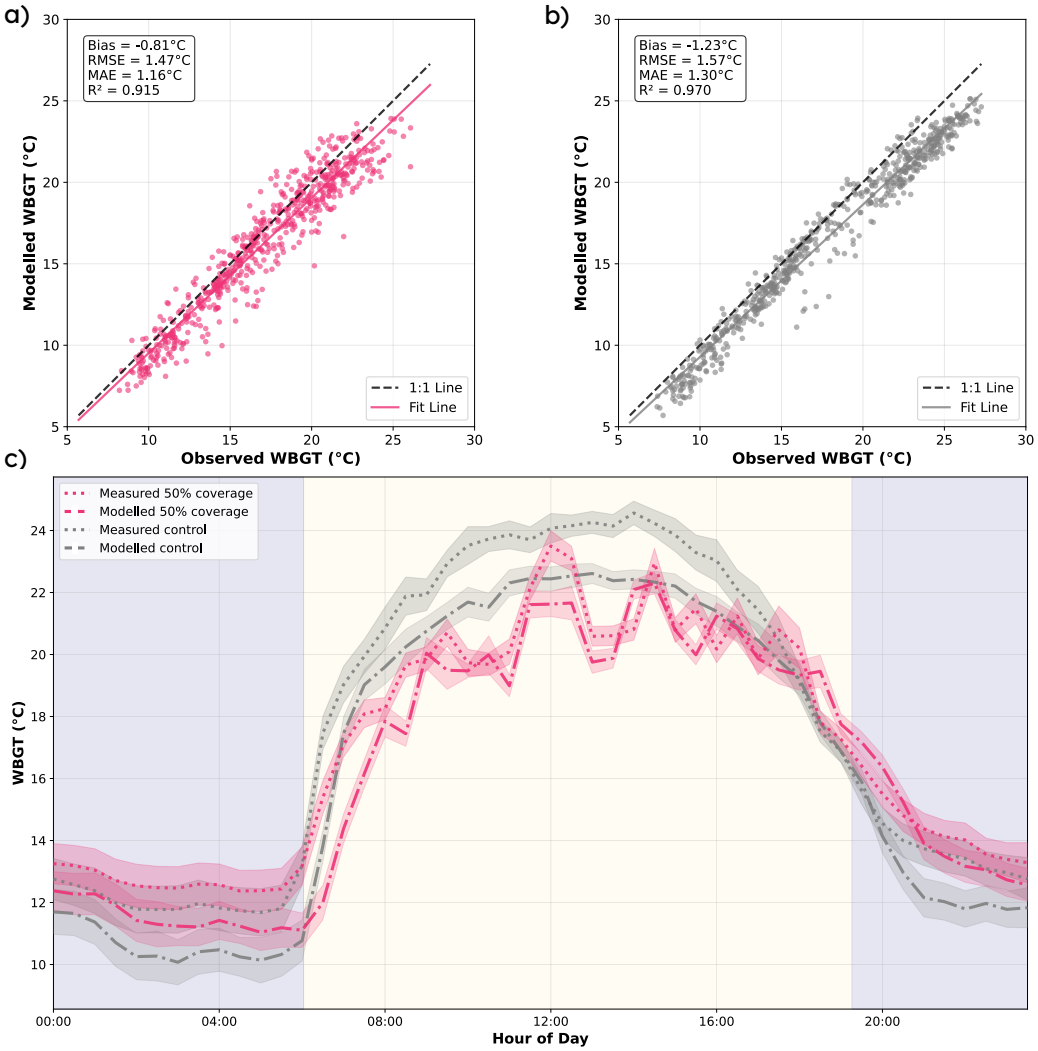

Figure S 8: Validation of modeled WBGT against observed values for the overhead agrivoltaic (pink) and respective control condition (grey). Scatter plots comparing modeled versus observed WBGT for a) 50% coverage, and b) control treatment, with performance statistics including bias, RMSE, MAE, and coefficient of determination (R^2). The dashed line represents perfect agreement (1:1 line) and the colored line shows the linear regression fit. C) shows diurnal patterns of observed and modeled WBGT showing temporal agreement between observations and predictions for both treatments, with shaded areas indicating variability ranges. Both treatments show negative bias (-0.81 °C 50% coverage, -1.23 °C control), consistent with known tendency of Kestrel instruments to read slightly high , particularly in direct sunlight/ low wind conditions. The models demonstrate strong correlations and effectively capture the diurnal patterns across both conditions. Data date range: 23rd May to 7th June 2025.

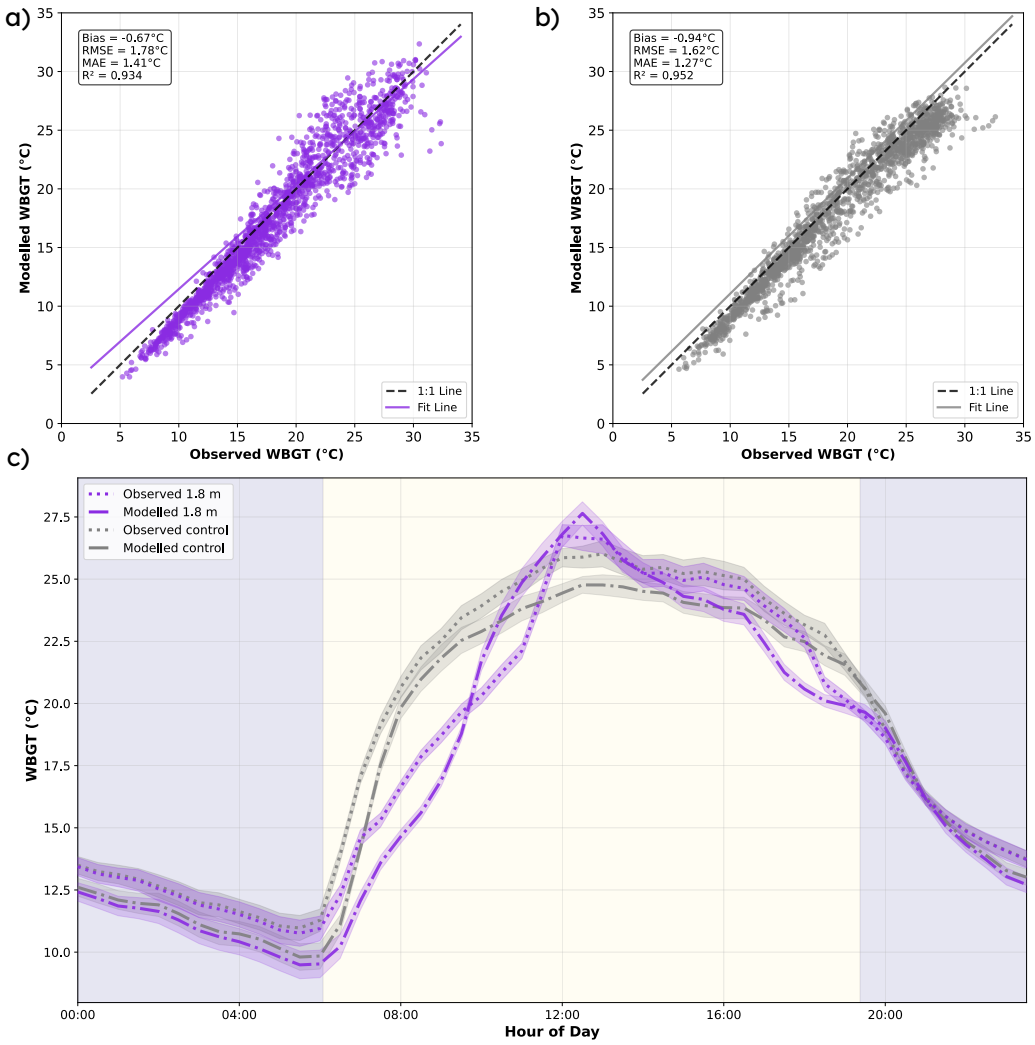

Figure S 9: Validation of modeled WBGT against observed values for the interspaced agrivoltaic (purple) and respective control condition (grey). Scatter plots comparing modeled versus observed WBGT for a) 1.8 m height, and b) control treatment, with performance statistics including bias, RMSE, MAE, and coefficient of determination (R^2). The dashed line represents perfect agreement (1:1 line) and the colored line shows the linear regression fit. C) shows diurnal patterns of observed and modeled WBGT showing temporal agreement between observations and predictions for both treatments, with shaded areas indicating variability ranges. Both treatments show negative bias (-0.67 °C 1.8 m, -0.94 °C control), consistent with known tendency of Kestrel instruments to read slightly high , particularly in direct sunlight conditions with low wind. The models demonstrate strong correlations and effectively capture the diurnal patterns across both conditions. Data date range: 16 Th June to 22nd July 2025.

Table S 1: Statistical significance of air temperature, relative humidity, wind speed, and solar radiation categorized by day and night for the raised overhead system (100% and 50% coverage) and the raised interspaced system (1.8 m and 2.4 m)

Treatment	Season	Variable	Time period	Absolute diff.	Percentage diff.	Sig. level
100%	Peak	Air temperature	Day	-0.47	-1.53	***
100%	Peak	Air temperature	Night	0.47	1.89	***
100%	Shoulder	Air temperature	Day	-0.56	-2.18	***
100%	Shoulder	Air temperature	Night	0.56	3.00	***
100%	Peak	Relative humidity	Day	2.25	7.51	***
100%	Peak	Relative humidity	Night	-1.40	-3.21	*
100%	Shoulder	Relative humidity	Day	2.38	12.37	***
100%	Shoulder	Relative humidity	Night	-1.62	-5.14	***
100%	Peak	Solar radiation	Day	-483.99	-86.65	***
100%	Shoulder	Solar radiation	Day	-498.79	-89.31	***
50%	Peak	Air temperature	Day	-0.50	-1.55	***
50%	Peak	Air temperature	Night	0.40	1.61	***
50%	Shoulder	Air temperature	Day	-0.46	-1.84	***
50%	Shoulder	Air temperature	Night	0.47	2.62	***
50%	Peak	Relative humidity	Day	1.50	6.36	***
50%	Peak	Relative humidity	Night	0.08	0.23	ns
50%	Shoulder	Relative humidity	Day	1.89	9.46	***
50%	Shoulder	Relative humidity	Night	-0.03	-0.08	ns
50%	Peak	Solar radiation	Day	-372.52	-64.73	***
50%	Shoulder	Solar radiation	Day	-358.15	-66.90	***
50%	Peak	Wind speed	Day	-0.15	-10.60	***
50%	Peak	Wind speed	Night	0.03	7.40	***
50%	Shoulder	Wind speed	Day	-0.20	-12.47	***

Continued on next page

Table S 1 – *Continued from previous page*

Treatment	Season	Variable	Time period	Absolute diff.	Percentage diff.	Sig. level
50%	Shoulder	Wind speed	Night	0.01	2.19	***
1.8 m	Peak	Air temperature	Day	-0.46	-1.80	**
1.8 m	Peak	Air temperature	Night	-0.40	-2.51	***
1.8 m	Shoulder	Air temperature	Day	-0.67	-3.67	***
1.8 m	Shoulder	Air temperature	Night	-0.43	-5.21	***
1.8 m	Peak	Relative humidity	Day	2.64	5.78	***
1.8 m	Peak	Relative humidity	Night	3.45	4.42	***
1.8 m	Shoulder	Relative humidity	Day	2.79	6.77	***
1.8 m	Shoulder	Relative humidity	Night	3.52	4.79	***
1.8 m	Peak	Solar radiation	Day	-93.29	-24.66	***
1.8 m	Shoulder	Solar radiation	Day	-94.97	-27.36	***
1.8 m	Peak	Wind speed	Day	-0.26	-27.90	***
1.8 m	Peak	Wind speed	Night	-0.23	-53.19	***
1.8 m	Shoulder	Wind speed	Day	-0.46	-36.63	***
1.8 m	Shoulder	Wind speed	Night	-0.36	-59.31	***
2.4 m	Peak	Air temperature	Day	-0.90	-3.53	***
2.4 m	Peak	Air temperature	Night	-0.37	-2.32	***
2.4 m	Shoulder	Air temperature	Day	-1.18	-6.42	***
2.4 m	Shoulder	Air temperature	Night	-0.45	-5.49	***
2.4 m	Peak	Relative humidity	Day	2.61	5.72	***
2.4 m	Peak	Relative humidity	Night	2.23	2.86	***
2.4 m	Shoulder	Relative humidity	Day	3.34	8.11	***
2.4 m	Shoulder	Relative humidity	Night	2.50	3.40	***
2.4 m	Peak	Solar radiation	Day	-106.70	-28.21	***
2.4 m	Shoulder	Solar radiation	Day	-103.64	-29.86	***

Table S 2: Summary table of globe temperature results including absolute and percentage difference between the named treatment and their respective full sun control, the significance (corrected using FDR), and the effect size.

Treatment	Season	Time	Absolute diff.	Percentage diff.	Sig.	Effect size
50% coverage	Peak	0:00	1.40	6.10	***	0.29
50% coverage	Peak	0:30	1.37	6.08	***	0.28
50% coverage	Peak	1:00	1.47	6.62	***	0.29
50% coverage	Peak	1:30	1.46	6.70	***	0.26
50% coverage	Peak	2:00	1.47	6.83	***	0.28
50% coverage	Peak	2:30	1.41	6.62	***	0.27
50% coverage	Peak	3:00	1.48	7.01	***	0.30
50% coverage	Peak	3:30	1.44	6.93	***	0.30
50% coverage	Peak	4:00	1.43	6.91	***	0.29
50% coverage	Peak	4:30	1.45	7.07	***	0.28
50% coverage	Peak	5:00	1.44	7.04	***	0.27
50% coverage	Peak	5:30	1.42	7.01	***	0.28
50% coverage	Peak	6:00	1.08	5.21	***	0.23
50% coverage	Peak	6:30	-1.12	-4.70	***	-0.26
50% coverage	Peak	7:00	-3.72	-12.32	***	-0.57
50% coverage	Peak	7:30	-5.57	-16.07	***	-0.67
50% coverage	Peak	8:00	-6.14	-16.44	***	-0.67
50% coverage	Peak	8:30	-5.59	-14.56	***	-0.64
50% coverage	Peak	9:00	-6.95	-17.26	***	-0.79
50% coverage	Peak	9:30	-7.30	-17.70	***	-0.84
50% coverage	Peak	10:00	-6.52	-15.49	***	-0.81
50% coverage	Peak	10:30	-4.81	-11.29	***	-0.62
50% coverage	Peak	11:00	-2.89	-6.71	***	-0.45
50% coverage	Peak	11:30	-4.11	-9.46	***	-0.59
50% coverage	Peak	12:00	-7.29	-16.52	***	-0.87
50% coverage	Peak	12:30	-7.18	-16.15	***	-0.87
50% coverage	Peak	13:00	-3.96	-8.91	***	-0.59
50% coverage	Peak	13:30	-2.20	-4.95	***	-0.34
50% coverage	Peak	14:00	-2.09	-4.70	***	-0.29
50% coverage	Peak	14:30	-4.35	-9.87	***	-0.60
50% coverage	Peak	15:00	-6.25	-14.31	***	-0.71
50% coverage	Peak	15:30	-5.76	-13.43	***	-0.67
50% coverage	Peak	16:00	-5.11	-11.95	***	-0.61
50% coverage	Peak	16:30	-4.26	-10.01	***	-0.55
50% coverage	Peak	17:00	-4.98	-11.92	***	-0.61
50% coverage	Peak	17:30	-3.08	-7.63	***	-0.41
50% coverage	Peak	18:00	-0.65	-1.70	ns	-0.09
50% coverage	Peak	18:30	1.92	5.72	***	0.26
50% coverage	Peak	19:00	2.70	8.94	***	0.41

Continued on next page

Table S 2 – *Continued from previous page*

Treatment	Season	Time	Absolute diff.	Percentage diff.	Sig.	Effect size
50% coverage	Peak	19:30	1.76	6.17	***	0.32
50% coverage	Peak	20:00	2.41	9.16	***	0.42
50% coverage	Peak	20:30	2.19	8.77	***	0.39
50% coverage	Peak	21:00	1.90	7.87	***	0.35
50% coverage	Peak	21:30	1.58	6.65	***	0.30
50% coverage	Peak	22:00	1.41	5.99	***	0.28
50% coverage	Peak	22:30	1.32	5.62	***	0.28
50% coverage	Peak	23:00	1.29	5.51	***	0.27
50% coverage	Peak	23:30	1.28	5.50	***	0.27
50% coverage	Shoulder	0:00	1.69	10.33	*	0.17
50% coverage	Shoulder	0:30	1.73	10.78	ns	0.16
50% coverage	Shoulder	1:00	1.67	10.58	ns	0.16
50% coverage	Shoulder	1:30	1.73	11.07	ns	0.16
50% coverage	Shoulder	2:00	1.76	11.48	*	0.17
50% coverage	Shoulder	2:30	1.69	11.16	ns	0.16
50% coverage	Shoulder	3:00	1.79	11.98	*	0.18
50% coverage	Shoulder	3:30	1.66	11.16	ns	0.16
50% coverage	Shoulder	4:00	1.68	11.38	ns	0.16
50% coverage	Shoulder	4:30	1.73	11.81	ns	0.17
50% coverage	Shoulder	5:00	1.72	11.87	ns	0.16
50% coverage	Shoulder	5:30	1.71	11.83	ns	0.16
50% coverage	Shoulder	6:00	1.57	10.83	ns	0.15
50% coverage	Shoulder	6:30	0.43	2.69	ns	0.03
50% coverage	Shoulder	7:00	-2.21	-10.79	**	-0.20
50% coverage	Shoulder	7:30	-3.40	-14.14	***	-0.32
50% coverage	Shoulder	8:00	-5.37	-18.44	***	-0.46
50% coverage	Shoulder	8:30	-6.13	-19.12	***	-0.47
50% coverage	Shoulder	9:00	-6.66	-19.33	***	-0.57
50% coverage	Shoulder	9:30	-6.38	-18.25	***	-0.52
50% coverage	Shoulder	10:00	-6.18	-17.63	***	-0.55
50% coverage	Shoulder	10:30	-6.10	-16.96	***	-0.52
50% coverage	Shoulder	11:00	-2.61	-7.13	**	-0.25
50% coverage	Shoulder	11:30	-3.77	-10.23	***	-0.35
50% coverage	Shoulder	12:00	-6.90	-18.48	***	-0.57
50% coverage	Shoulder	12:30	-6.58	-17.54	***	-0.54
50% coverage	Shoulder	13:00	-4.27	-11.27	***	-0.40
50% coverage	Shoulder	13:30	-3.34	-8.79	***	-0.30
50% coverage	Shoulder	14:00	-3.30	-8.67	***	-0.30
50% coverage	Shoulder	14:30	-4.27	-11.23	***	-0.39
50% coverage	Shoulder	15:00	-5.79	-15.49	***	-0.52
50% coverage	Shoulder	15:30	-5.54	-15.05	***	-0.49
50% coverage	Shoulder	16:00	-3.23	-8.80	***	-0.29
50% coverage	Shoulder	16:30	-4.34	-12.02	***	-0.42

Continued on next page

Table S 2 – *Continued from previous page*

Treatment	Season	Time	Absolute diff.	Percentage diff.	Sig.	Effect size
50% coverage	Shoulder	17:00	-4.19	-11.97	***	-0.37
50% coverage	Shoulder	17:30	-1.48	-4.62	ns	-0.16
50% coverage	Shoulder	18:00	1.81	6.48	ns	0.16
50% coverage	Shoulder	18:30	3.75	15.74	***	0.37
50% coverage	Shoulder	19:00	2.34	10.62	***	0.26
50% coverage	Shoulder	19:30	2.52	12.44	***	0.28
50% coverage	Shoulder	20:00	2.50	13.27	***	0.27
50% coverage	Shoulder	20:30	2.30	12.69	**	0.23
50% coverage	Shoulder	21:00	2.03	11.48	*	0.19
50% coverage	Shoulder	21:30	1.82	10.45	*	0.17
50% coverage	Shoulder	22:00	1.66	9.55	ns	0.16
50% coverage	Shoulder	22:30	1.75	10.25	ns	0.16
50% coverage	Shoulder	23:00	1.74	10.34	ns	0.17
50% coverage	Shoulder	23:30	1.73	10.48	ns	0.17
1.8 m	Peak	0:00	-0.30	-1.80	ns	-0.06
1.8 m	Peak	0:30	-0.34	-2.08	ns	-0.07
1.8 m	Peak	1:00	-0.31	-1.98	ns	-0.07
1.8 m	Peak	1:30	-0.36	-2.36	ns	-0.08
1.8 m	Peak	2:00	-0.39	-2.62	ns	-0.08
1.8 m	Peak	2:30	-0.40	-2.81	ns	-0.08
1.8 m	Peak	3:00	-0.45	-3.26	ns	-0.10
1.8 m	Peak	3:30	-0.43	-3.20	ns	-0.09
1.8 m	Peak	4:00	-0.45	-3.47	ns	-0.09
1.8 m	Peak	4:30	-0.46	-3.62	ns	-0.10
1.8 m	Peak	5:00	-0.46	-3.68	ns	-0.10
1.8 m	Peak	5:30	-0.47	-3.88	ns	-0.11
1.8 m	Peak	6:00	-0.47	-3.96	ns	-0.10
1.8 m	Peak	6:30	-0.46	-3.96	ns	-0.10
1.8 m	Peak	7:00	-0.51	-4.33	ns	-0.11
1.8 m	Peak	7:30	-1.69	-12.65	***	-0.34
1.8 m	Peak	8:00	-3.93	-23.11	***	-0.55
1.8 m	Peak	8:30	-6.39	-29.52	***	-0.74
1.8 m	Peak	9:00	-7.92	-31.04	***	-0.78
1.8 m	Peak	9:30	-8.09	-28.78	***	-0.75
1.8 m	Peak	10:00	-5.96	-19.69	***	-0.60
1.8 m	Peak	10:30	-2.01	-6.30	***	-0.23
1.8 m	Peak	11:00	-0.29	-0.88	ns	-0.03
1.8 m	Peak	11:30	0.21	0.62	ns	0.03
1.8 m	Peak	12:00	0.74	2.13	ns	0.09
1.8 m	Peak	12:30	1.38	3.91	*	0.17
1.8 m	Peak	13:00	2.05	5.73	***	0.24
1.8 m	Peak	13:30	2.13	5.83	***	0.27
1.8 m	Peak	14:00	1.68	4.53	**	0.20

Continued on next page

Table S 2 – *Continued from previous page*

Treatment	Season	Time	Absolute diff.	Percentage diff.	Sig.	Effect size
1.8 m	Peak	14:30	1.05	2.82	ns	0.13
1.8 m	Peak	15:00	0.49	1.33	ns	0.07
1.8 m	Peak	15:30	0.37	1.02	ns	0.05
1.8 m	Peak	16:00	0.01	0.02	ns	0.00
1.8 m	Peak	16:30	-0.22	-0.62	ns	-0.02
1.8 m	Peak	17:00	-0.30	-0.85	ns	-0.03
1.8 m	Peak	17:30	-0.29	-0.85	ns	-0.03
1.8 m	Peak	18:00	-0.49	-1.47	ns	-0.05
1.8 m	Peak	18:30	-1.45	-4.40	ns	-0.14
1.8 m	Peak	19:00	-2.93	-9.21	***	-0.29
1.8 m	Peak	19:30	-3.65	-11.83	***	-0.37
1.8 m	Peak	20:00	-3.72	-12.53	***	-0.37
1.8 m	Peak	20:30	-2.98	-10.88	***	-0.33
1.8 m	Peak	21:00	-1.88	-7.69	**	-0.20
1.8 m	Peak	21:30	-0.67	-3.11	ns	-0.10
1.8 m	Peak	22:00	-0.26	-1.34	ns	-0.05
1.8 m	Peak	22:30	-0.28	-1.53	ns	-0.06
1.8 m	Peak	23:00	-0.30	-1.70	ns	-0.06
1.8 m	Peak	23:30	-0.30	-1.75	ns	-0.06
1.8 m	Shoulder	0:00	-0.50	-5.87	ns	-0.07
1.8 m	Shoulder	0:30	-0.52	-6.45	ns	-0.07
1.8 m	Shoulder	1:00	-0.51	-6.82	ns	-0.07
1.8 m	Shoulder	1:30	-0.52	-7.32	ns	-0.07
1.8 m	Shoulder	2:00	-0.50	-7.63	ns	-0.07
1.8 m	Shoulder	2:30	-0.53	-8.52	ns	-0.07
1.8 m	Shoulder	3:00	-0.51	-8.73	ns	-0.07
1.8 m	Shoulder	3:30	-0.51	-9.15	ns	-0.07
1.8 m	Shoulder	4:00	-0.50	-9.35	ns	-0.07
1.8 m	Shoulder	4:30	-0.50	-9.75	ns	-0.07
1.8 m	Shoulder	5:00	-0.49	-9.96	ns	-0.07
1.8 m	Shoulder	5:30	-0.45	-9.87	ns	-0.06
1.8 m	Shoulder	6:00	-0.46	-10.47	ns	-0.06
1.8 m	Shoulder	6:30	-0.45	-11.12	ns	-0.06
1.8 m	Shoulder	7:00	-0.48	-12.60	ns	-0.07
1.8 m	Shoulder	7:30	-0.85	-19.99	*	-0.12
1.8 m	Shoulder	8:00	-1.95	-32.82	***	-0.22
1.8 m	Shoulder	8:30	-3.92	-42.22	***	-0.34
1.8 m	Shoulder	9:00	-6.57	-46.99	***	-0.53
1.8 m	Shoulder	9:30	-8.16	-45.60	***	-0.63
1.8 m	Shoulder	10:00	-7.71	-37.32	***	-0.58
1.8 m	Shoulder	10:30	-5.34	-23.54	***	-0.40
1.8 m	Shoulder	11:00	-1.61	-6.77	*	-0.12
1.8 m	Shoulder	11:30	-0.11	-0.43	ns	0.00

Continued on next page

Table S 2 – *Continued from previous page*

Treatment	Season	Time	Absolute diff.	Percentage diff.	Sig.	Effect size
1.8 m	Shoulder	12:00	0.30	1.17	ns	0.03
1.8 m	Shoulder	12:30	0.58	2.19	ns	0.05
1.8 m	Shoulder	13:00	0.90	3.30	ns	0.08
1.8 m	Shoulder	13:30	1.06	3.80	ns	0.10
1.8 m	Shoulder	14:00	0.79	2.80	ns	0.06
1.8 m	Shoulder	14:30	0.43	1.52	ns	0.04
1.8 m	Shoulder	15:00	0.22	0.76	ns	0.01
1.8 m	Shoulder	15:30	-0.02	-0.07	ns	0.00
1.8 m	Shoulder	16:00	-0.25	-0.86	ns	-0.02
1.8 m	Shoulder	16:30	-0.50	-1.76	ns	-0.04
1.8 m	Shoulder	17:00	-0.71	-2.55	ns	-0.06
1.8 m	Shoulder	17:30	-1.41	-5.15	ns	-0.11
1.8 m	Shoulder	18:00	-2.69	-10.06	***	-0.21
1.8 m	Shoulder	18:30	-3.70	-14.69	***	-0.27
1.8 m	Shoulder	19:00	-4.16	-17.55	***	-0.31
1.8 m	Shoulder	19:30	-3.60	-16.72	***	-0.27
1.8 m	Shoulder	20:00	-2.38	-12.89	***	-0.20
1.8 m	Shoulder	20:30	-1.39	-8.99	*	-0.12
1.8 m	Shoulder	21:00	-0.79	-6.08	ns	-0.08
1.8 m	Shoulder	21:30	-0.52	-4.57	ns	-0.06
1.8 m	Shoulder	22:00	-0.47	-4.38	ns	-0.06
1.8 m	Shoulder	22:30	-0.46	-4.59	ns	-0.06
1.8 m	Shoulder	23:00	-0.45	-4.78	ns	-0.06
1.8 m	Shoulder	23:30	-0.48	-5.28	ns	-0.06
2.4 m	Peak	0:00	-0.23	-1.37	ns	-0.05
2.4 m	Peak	0:30	-0.28	-1.73	ns	-0.06
2.4 m	Peak	1:00	-0.27	-1.69	ns	-0.06
2.4 m	Peak	1:30	-0.31	-2.01	ns	-0.07
2.4 m	Peak	2:00	-0.32	-2.15	ns	-0.07
2.4 m	Peak	2:30	-0.32	-2.26	ns	-0.07
2.4 m	Peak	3:00	-0.42	-2.98	ns	-0.09
2.4 m	Peak	3:30	-0.38	-2.80	ns	-0.08
2.4 m	Peak	4:00	-0.41	-3.12	ns	-0.08
2.4 m	Peak	4:30	-0.43	-3.32	ns	-0.09
2.4 m	Peak	5:00	-0.41	-3.30	ns	-0.09
2.4 m	Peak	5:30	-0.44	-3.62	ns	-0.10
2.4 m	Peak	6:00	-0.44	-3.66	ns	-0.09
2.4 m	Peak	6:30	-0.44	-3.72	ns	-0.09
2.4 m	Peak	7:00	-0.50	-4.22	ns	-0.11
2.4 m	Peak	7:30	-1.58	-11.81	***	-0.33
2.4 m	Peak	8:00	-2.61	-15.33	***	-0.36
2.4 m	Peak	8:30	-5.96	-27.54	***	-0.71
2.4 m	Peak	9:00	-7.91	-31.01	***	-0.80

Continued on next page

Table S 2 – *Continued from previous page*

Treatment	Season	Time	Absolute diff.	Percentage diff.	Sig.	Effect size
2.4 m	Peak	9:30	-8.34	-29.67	***	-0.77
2.4 m	Peak	10:00	-8.38	-27.70	***	-0.77
2.4 m	Peak	10:30	-7.41	-23.17	***	-0.73
2.4 m	Peak	11:00	-3.07	-9.17	***	-0.33
2.4 m	Peak	11:30	-0.33	-0.95	ns	-0.03
2.4 m	Peak	12:00	0.36	1.03	ns	0.04
2.4 m	Peak	12:30	1.04	2.94	ns	0.13
2.4 m	Peak	13:00	1.66	4.62	**	0.19
2.4 m	Peak	13:30	1.60	4.38	**	0.21
2.4 m	Peak	14:00	1.16	3.13	ns	0.14
2.4 m	Peak	14:30	0.62	1.66	ns	0.09
2.4 m	Peak	15:00	0.13	0.36	ns	0.03
2.4 m	Peak	15:30	0.05	0.15	ns	0.01
2.4 m	Peak	16:00	-0.19	-0.54	ns	-0.02
2.4 m	Peak	16:30	-0.33	-0.95	ns	-0.03
2.4 m	Peak	17:00	-0.43	-1.23	ns	-0.04
2.4 m	Peak	17:30	-0.59	-1.72	ns	-0.05
2.4 m	Peak	18:00	-1.75	-5.21	*	-0.17
2.4 m	Peak	18:30	-3.58	-10.87	***	-0.35
2.4 m	Peak	19:00	-4.01	-12.60	***	-0.40
2.4 m	Peak	19:30	-3.94	-12.77	***	-0.40
2.4 m	Peak	20:00	-3.77	-12.69	***	-0.37
2.4 m	Peak	20:30	-2.97	-10.86	***	-0.32
2.4 m	Peak	21:00	-1.22	-4.98	ns	-0.13
2.4 m	Peak	21:30	-0.73	-3.42	ns	-0.11
2.4 m	Peak	22:00	-0.19	-0.96	ns	-0.04
2.4 m	Peak	22:30	-0.19	-1.00	ns	-0.04
2.4 m	Peak	23:00	-0.25	-1.38	ns	-0.06
2.4 m	Peak	23:30	-0.24	-1.40	ns	-0.05
2.4 m	Shoulder	0:00	-0.37	-4.32	ns	-0.05
2.4 m	Shoulder	0:30	-0.37	-4.65	ns	-0.05
2.4 m	Shoulder	1:00	-0.38	-5.04	ns	-0.05
2.4 m	Shoulder	1:30	-0.38	-5.42	ns	-0.05
2.4 m	Shoulder	2:00	-0.37	-5.65	ns	-0.05
2.4 m	Shoulder	2:30	-0.40	-6.41	ns	-0.06
2.4 m	Shoulder	3:00	-0.39	-6.80	ns	-0.06
2.4 m	Shoulder	3:30	-0.41	-7.44	ns	-0.06
2.4 m	Shoulder	4:00	-0.39	-7.43	ns	-0.06
2.4 m	Shoulder	4:30	-0.40	-7.83	ns	-0.06
2.4 m	Shoulder	5:00	-0.41	-8.38	ns	-0.06
2.4 m	Shoulder	5:30	-0.37	-8.07	ns	-0.05
2.4 m	Shoulder	6:00	-0.37	-8.55	ns	-0.05
2.4 m	Shoulder	6:30	-0.36	-8.86	ns	-0.05

Continued on next page

Table S 2 – *Continued from previous page*

Treatment	Season	Time	Absolute diff.	Percentage diff.	Sig.	Effect size
2.4 m	Shoulder	7:00	-0.40	-10.39	ns	-0.06
2.4 m	Shoulder	7:30	-0.68	-15.88	ns	-0.10
2.4 m	Shoulder	8:00	-1.49	-25.11	**	-0.16
2.4 m	Shoulder	8:30	-3.71	-39.98	***	-0.32
2.4 m	Shoulder	9:00	-6.08	-43.50	***	-0.49
2.4 m	Shoulder	9:30	-7.91	-44.22	***	-0.62
2.4 m	Shoulder	10:00	-8.51	-41.15	***	-0.64
2.4 m	Shoulder	10:30	-7.89	-34.82	***	-0.60
2.4 m	Shoulder	11:00	-5.29	-22.23	***	-0.42
2.4 m	Shoulder	11:30	-1.97	-7.93	**	-0.15
2.4 m	Shoulder	12:00	0.05	0.19	ns	0.01
2.4 m	Shoulder	12:30	0.38	1.45	ns	0.04
2.4 m	Shoulder	13:00	0.76	2.78	ns	0.07
2.4 m	Shoulder	13:30	0.70	2.50	ns	0.07
2.4 m	Shoulder	14:00	0.28	0.99	ns	0.02
2.4 m	Shoulder	14:30	0.03	0.09	ns	0.01
2.4 m	Shoulder	15:00	-0.12	-0.40	ns	-0.01
2.4 m	Shoulder	15:30	-0.16	-0.56	ns	-0.01
2.4 m	Shoulder	16:00	-0.21	-0.73	ns	-0.02
2.4 m	Shoulder	16:30	-0.61	-2.16	ns	-0.05
2.4 m	Shoulder	17:00	-1.51	-5.40	ns	-0.11
2.4 m	Shoulder	17:30	-2.58	-9.44	***	-0.21
2.4 m	Shoulder	18:00	-4.28	-16.01	***	-0.32
2.4 m	Shoulder	18:30	-4.58	-18.17	***	-0.34
2.4 m	Shoulder	19:00	-4.19	-17.66	***	-0.32
2.4 m	Shoulder	19:30	-3.46	-16.06	***	-0.25
2.4 m	Shoulder	20:00	-2.13	-11.55	***	-0.18
2.4 m	Shoulder	20:30	-1.21	-7.81	ns	-0.10
2.4 m	Shoulder	21:00	-0.50	-3.86	ns	-0.05
2.4 m	Shoulder	21:30	-0.36	-3.14	ns	-0.04
2.4 m	Shoulder	22:00	-0.32	-3.00	ns	-0.04
2.4 m	Shoulder	22:30	-0.32	-3.17	ns	-0.04
2.4 m	Shoulder	23:00	-0.30	-3.19	ns	-0.04
2.4 m	Shoulder	23:30	-0.35	-3.84	ns	-0.05

Table S 3: Summary table for wet bulb globe temperature differences between agrivoltaic treatments and their respective control. The table includes each 30-minute interval, absolute difference and percentage difference between each agrivoltaic treatment and control condition, the significance of the difference (corrected for FDR), and the effect size.

Treatment	Season	Time	Absolute diff.	Percentage diff.	Sig.	Effect size
100% coverage	Peak	0:00	0.43	2.49	ns	0.07
100% coverage	Peak	0:30	0.41	2.40	ns	0.07
100% coverage	Peak	1:00	0.44	2.58	ns	0.07
100% coverage	Peak	1:30	0.45	2.69	ns	0.08
100% coverage	Peak	2:00	0.46	2.74	ns	0.07
100% coverage	Peak	2:30	0.46	2.77	ns	0.08
100% coverage	Peak	3:00	0.48	2.96	ns	0.08
100% coverage	Peak	3:30	0.48	2.92	ns	0.08
100% coverage	Peak	4:00	0.50	3.07	*	0.09
100% coverage	Peak	4:30	0.47	2.95	ns	0.08
100% coverage	Peak	5:00	0.41	2.56	ns	0.07
100% coverage	Peak	5:30	0.44	2.73	ns	0.08
100% coverage	Peak	6:00	0.13	0.79	ns	0.02
100% coverage	Peak	6:30	-0.62	-3.57	**	-0.14
100% coverage	Peak	7:00	-1.73	-8.93	***	-0.40
100% coverage	Peak	7:30	-2.38	-11.11	***	-0.53
100% coverage	Peak	8:00	-2.75	-12.15	***	-0.60
100% coverage	Peak	8:30	-3.04	-12.93	***	-0.65
100% coverage	Peak	9:00	-2.32	-9.74	***	-0.51

Continued on next page

Table S 3 – *Continued from previous page*

Treatment	Season	Time	Absolute diff.	Percentage diff.	Sig.	Effect size
100% coverage	Peak	9:30	-2.38	-9.82	***	-0.55
100% coverage	Peak	10:00	-2.72	-10.99	***	-0.63
100% coverage	Peak	10:30	-2.98	-11.86	***	-0.69
100% coverage	Peak	11:00	-3.01	-11.89	***	-0.70
100% coverage	Peak	11:30	-2.75	-10.74	***	-0.68
100% coverage	Peak	12:00	-2.75	-10.69	***	-0.68
100% coverage	Peak	12:30	-2.58	-10.00	***	-0.66
100% coverage	Peak	13:00	-2.56	-9.90	***	-0.66
100% coverage	Peak	13:30	-2.52	-9.71	***	-0.64
100% coverage	Peak	14:00	-2.29	-8.89	***	-0.56
100% coverage	Peak	14:30	-2.31	-9.02	***	-0.56
100% coverage	Peak	15:00	-2.19	-8.61	***	-0.53
100% coverage	Peak	15:30	-1.98	-7.86	***	-0.49
100% coverage	Peak	16:00	-1.92	-7.68	***	-0.48
100% coverage	Peak	16:30	-1.61	-6.55	***	-0.41
100% coverage	Peak	17:00	-1.29	-5.33	***	-0.34
100% coverage	Peak	17:30	-1.03	-4.33	***	-0.26
100% coverage	Peak	18:00	-0.50	-2.18	**	-0.14
100% coverage	Peak	18:30	0.32	1.51	ns	0.07
100% coverage	Peak	19:00	0.40	1.92	ns	0.08
100% coverage	Peak	19:30	0.61	3.08	**	0.14

Continued on next page

Table S 3 – *Continued from previous page*

Treatment	Season	Time	Absolute diff.	Percentage diff.	Sig.	Effect size
100% coverage	Peak	20:00	0.73	3.84	***	0.16
100% coverage	Peak	20:30	0.77	4.20	***	0.15
100% coverage	Peak	21:00	0.69	3.82	**	0.13
100% coverage	Peak	21:30	0.61	3.39	**	0.12
100% coverage	Peak	22:00	0.53	2.97	*	0.10
100% coverage	Peak	22:30	0.46	2.59	ns	0.08
100% coverage	Peak	23:00	0.46	2.61	ns	0.08
100% coverage	Peak	23:30	0.43	2.46	ns	0.07
100% coverage	Shoulder	0:00	0.66	7.16	*	0.11
100% coverage	Shoulder	0:30	0.63	7.08	*	0.11
100% coverage	Shoulder	1:00	0.63	7.17	*	0.11
100% coverage	Shoulder	1:30	0.61	7.10	*	0.11
100% coverage	Shoulder	2:00	0.62	7.33	*	0.11
100% coverage	Shoulder	2:30	0.66	8.05	*	0.12
100% coverage	Shoulder	3:00	0.67	8.34	*	0.12
100% coverage	Shoulder	3:30	0.62	7.89	*	0.12
100% coverage	Shoulder	4:00	0.64	8.18	*	0.12
100% coverage	Shoulder	4:30	0.62	8.07	*	0.12
100% coverage	Shoulder	5:00	0.62	8.15	*	0.12
100% coverage	Shoulder	5:30	0.58	7.50	*	0.11
100% coverage	Shoulder	6:00	0.36	4.56	ns	0.06

Continued on next page

Table S 3 – *Continued from previous page*

Treatment	Season	Time	Absolute diff.	Percentage diff.	Sig.	Effect size
100% coverage	Shoulder	6:30	-0.49	-5.36	ns	-0.09
100% coverage	Shoulder	7:00	-1.66	-14.29	***	-0.25
100% coverage	Shoulder	7:30	-2.44	-17.49	***	-0.35
100% coverage	Shoulder	8:00	-3.33	-21.14	***	-0.53
100% coverage	Shoulder	8:30	-2.91	-17.09	***	-0.49
100% coverage	Shoulder	9:00	-2.80	-16.11	***	-0.40
100% coverage	Shoulder	9:30	-3.01	-16.79	***	-0.46
100% coverage	Shoulder	10:00	-3.39	-18.46	***	-0.55
100% coverage	Shoulder	10:30	-3.48	-18.62	***	-0.58
100% coverage	Shoulder	11:00	-3.22	-17.17	***	-0.55
100% coverage	Shoulder	11:30	-3.02	-15.99	***	-0.52
100% coverage	Shoulder	12:00	-2.97	-15.83	***	-0.52
100% coverage	Shoulder	12:30	-2.77	-14.65	***	-0.49
100% coverage	Shoulder	13:00	-2.74	-14.39	***	-0.50
100% coverage	Shoulder	13:30	-2.71	-14.35	***	-0.49
100% coverage	Shoulder	14:00	-2.56	-13.20	***	-0.49
100% coverage	Shoulder	14:30	-2.64	-13.62	***	-0.50
100% coverage	Shoulder	15:00	-2.46	-12.81	***	-0.49
100% coverage	Shoulder	15:30	-2.23	-11.75	***	-0.45
100% coverage	Shoulder	16:00	-2.05	-10.99	***	-0.42
100% coverage	Shoulder	16:30	-1.73	-9.48	***	-0.36

Continued on next page

Table S 3 – *Continued from previous page*

Treatment	Season	Time	Absolute diff.	Percentage diff.	Sig.	Effect size
100% coverage	Shoulder	17:00	-1.33	-7.43	***	-0.26
100% coverage	Shoulder	17:30	-0.73	-4.30	**	-0.15
100% coverage	Shoulder	18:00	0.01	0.07	ns	0.00
100% coverage	Shoulder	18:30	0.83	5.87	**	0.16
100% coverage	Shoulder	19:00	0.70	5.27	**	0.14
100% coverage	Shoulder	19:30	0.98	8.04	***	0.19
100% coverage	Shoulder	20:00	1.06	9.44	***	0.21
100% coverage	Shoulder	20:30	1.05	10.02	***	0.20
100% coverage	Shoulder	21:00	0.88	8.71	**	0.16
100% coverage	Shoulder	21:30	0.73	7.32	*	0.12
100% coverage	Shoulder	22:00	0.58	5.84	ns	0.10
100% coverage	Shoulder	22:30	0.59	6.03	*	0.10
100% coverage	Shoulder	23:00	0.60	6.18	*	0.11
100% coverage	Shoulder	23:30	0.59	6.17	*	0.10
50% coverage	Peak	0:00	0.58	3.51	*	0.10
50% coverage	Peak	0:30	0.53	3.26	ns	0.08
50% coverage	Peak	1:00	0.61	3.83	ns	0.09
50% coverage	Peak	1:30	0.63	3.96	ns	0.09
50% coverage	Peak	2:00	0.64	4.12	ns	0.09
50% coverage	Peak	2:30	0.64	4.11	ns	0.10
50% coverage	Peak	3:00	0.65	4.19	*	0.10
50% coverage	Peak	3:30	0.62	4.07	ns	0.09
50% coverage	Peak	4:00	0.64	4.21	*	0.10
50% coverage	Peak	4:30	0.66	4.40	*	0.10
50% coverage	Peak	5:00	0.59	3.92	ns	0.10
50% coverage	Peak	5:30	0.58	3.84	*	0.10
50% coverage	Peak	6:00	0.32	2.07	ns	0.06
50% coverage	Peak	6:30	-0.59	-3.52	*	-0.12
50% coverage	Peak	7:00	-1.84	-9.39	***	-0.36

Continued on next page

Table S 3 – *Continued from previous page*

Treatment	Season	Time	Absolute diff.	Percentage diff.	Sig.	Effect size
50% coverage	Peak	7:30	-2.20	-10.12	***	-0.43
50% coverage	Peak	8:00	-2.20	-9.58	***	-0.45
50% coverage	Peak	8:30	-2.24	-9.48	***	-0.52
50% coverage	Peak	9:00	-1.66	-6.81	***	-0.38
50% coverage	Peak	9:30	-1.74	-7.22	***	-0.39
50% coverage	Peak	10:00	-2.06	-8.31	***	-0.47
50% coverage	Peak	10:30	-1.69	-6.77	***	-0.39
50% coverage	Peak	11:00	-2.16	-8.55	***	-0.47
50% coverage	Peak	11:30	-1.57	-6.12	***	-0.40
50% coverage	Peak	12:00	-1.60	-6.27	***	-0.40
50% coverage	Peak	12:30	-1.60	-6.17	***	-0.39
50% coverage	Peak	13:00	-1.83	-7.04	***	-0.44
50% coverage	Peak	13:30	-1.62	-6.25	***	-0.38
50% coverage	Peak	14:00	-0.88	-3.41	***	-0.22
50% coverage	Peak	14:30	-1.07	-4.19	***	-0.25
50% coverage	Peak	15:00	-1.90	-7.47	***	-0.42
50% coverage	Peak	15:30	-1.76	-6.99	***	-0.41
50% coverage	Peak	16:00	-0.90	-3.61	***	-0.23
50% coverage	Peak	16:30	-1.01	-4.08	***	-0.24
50% coverage	Peak	17:00	-1.15	-4.74	***	-0.27
50% coverage	Peak	17:30	-0.67	-2.85	**	-0.15
50% coverage	Peak	18:00	0.07	0.30	ns	0.01
50% coverage	Peak	18:30	0.67	3.13	**	0.14
50% coverage	Peak	19:00	0.80	3.96	***	0.17
50% coverage	Peak	19:30	0.77	3.99	**	0.15
50% coverage	Peak	20:00	1.10	6.03	***	0.20
50% coverage	Peak	20:30	1.00	5.71	***	0.18
50% coverage	Peak	21:00	0.88	5.12	**	0.15
50% coverage	Peak	21:30	0.75	4.44	**	0.13
50% coverage	Peak	22:00	0.63	3.75	*	0.11
50% coverage	Peak	22:30	0.59	3.52	*	0.10
50% coverage	Peak	23:00	0.58	3.47	ns	0.09
50% coverage	Peak	23:30	0.55	3.31	ns	0.09
50% coverage	Shoulder	0:00	0.58	6.35	ns	0.09
50% coverage	Shoulder	0:30	0.60	6.64	ns	0.10
50% coverage	Shoulder	1:00	0.61	6.96	ns	0.10
50% coverage	Shoulder	1:30	0.64	7.42	ns	0.10
50% coverage	Shoulder	2:00	0.62	7.43	*	0.10
50% coverage	Shoulder	2:30	0.61	7.43	*	0.10
50% coverage	Shoulder	3:00	0.64	7.83	*	0.10
50% coverage	Shoulder	3:30	0.58	7.11	ns	0.09
50% coverage	Shoulder	4:00	0.61	7.60	ns	0.10
50% coverage	Shoulder	4:30	0.63	8.05	ns	0.10

Continued on next page

Table S 3 – *Continued from previous page*

Treatment	Season	Time	Absolute diff.	Percentage diff.	Sig.	Effect size
50% coverage	Shoulder	5:00	0.62	7.96	ns	0.10
50% coverage	Shoulder	5:30	0.57	7.35	ns	0.09
50% coverage	Shoulder	6:00	0.46	5.81	ns	0.07
50% coverage	Shoulder	6:30	-0.34	-3.77	ns	-0.06
50% coverage	Shoulder	7:00	-1.39	-12.17	***	-0.21
50% coverage	Shoulder	7:30	-2.06	-14.93	***	-0.31
50% coverage	Shoulder	8:00	-2.43	-15.47	***	-0.39
50% coverage	Shoulder	8:30	-1.99	-11.68	***	-0.34
50% coverage	Shoulder	9:00	-1.67	-9.54	***	-0.27
50% coverage	Shoulder	9:30	-1.85	-10.13	***	-0.29
50% coverage	Shoulder	10:00	-1.96	-10.61	***	-0.30
50% coverage	Shoulder	10:30	-1.94	-10.39	***	-0.33
50% coverage	Shoulder	11:00	-2.71	-14.47	***	-0.43
50% coverage	Shoulder	11:30	-1.57	-8.37	***	-0.24
50% coverage	Shoulder	12:00	-1.18	-6.10	***	-0.20
50% coverage	Shoulder	12:30	-0.97	-5.10	**	-0.15
50% coverage	Shoulder	13:00	-1.79	-9.43	***	-0.30
50% coverage	Shoulder	13:30	-1.68	-8.84	***	-0.29
50% coverage	Shoulder	14:00	-1.10	-5.75	***	-0.19
50% coverage	Shoulder	14:30	-1.33	-6.94	***	-0.23
50% coverage	Shoulder	15:00	-2.02	-10.70	***	-0.36
50% coverage	Shoulder	15:30	-1.64	-8.81	***	-0.30
50% coverage	Shoulder	16:00	-0.58	-3.09	*	-0.11
50% coverage	Shoulder	16:30	-0.98	-5.48	***	-0.19
50% coverage	Shoulder	17:00	-1.26	-7.15	***	-0.23
50% coverage	Shoulder	17:30	-0.43	-2.59	ns	-0.09
50% coverage	Shoulder	18:00	0.45	2.93	ns	0.08
50% coverage	Shoulder	18:30	1.01	7.44	***	0.19
50% coverage	Shoulder	19:00	0.82	6.51	**	0.15
50% coverage	Shoulder	19:30	1.09	9.40	***	0.19
50% coverage	Shoulder	20:00	1.13	10.62	***	0.20
50% coverage	Shoulder	20:30	1.02	10.11	***	0.17
50% coverage	Shoulder	21:00	0.90	9.10	**	0.14
50% coverage	Shoulder	21:30	0.66	6.72	*	0.11
50% coverage	Shoulder	22:00	0.58	5.96	ns	0.09
50% coverage	Shoulder	22:30	0.60	6.13	ns	0.09
50% coverage	Shoulder	23:00	0.59	6.26	ns	0.09
50% coverage	Shoulder	23:30	0.59	6.27	ns	0.09
1.8 m	Peak	0:00	-0.21	-1.52	ns	-0.08
1.8 m	Peak	0:30	-0.28	-2.02	ns	-0.06
1.8 m	Peak	1:00	-0.30	-2.21	ns	-0.07
1.8 m	Peak	1:30	-0.26	-2.02	ns	-0.08
1.8 m	Peak	2:00	-0.35	-2.77	ns	-0.06

Continued on next page

Table S 3 – *Continued from previous page*

Treatment	Season	Time	Absolute diff.	Percentage diff.	Sig.	Effect size
1.8 m	Peak	2:30	-0.33	-2.67	ns	-0.08
1.8 m	Peak	3:00	-0.37	-3.02	ns	-0.08
1.8 m	Peak	3:30	-0.41	-3.43	ns	-0.09
1.8 m	Peak	4:00	-0.37	-3.21	ns	-0.09
1.8 m	Peak	4:30	-0.38	-3.43	ns	-0.08
1.8 m	Peak	5:00	-0.37	-3.39	ns	-0.09
1.8 m	Peak	5:30	-0.40	-3.73	ns	-0.08
1.8 m	Peak	6:00	-0.41	-3.88	ns	-0.09
1.8 m	Peak	6:30	-0.40	-3.89	ns	-0.09
1.8 m	Peak	7:00	-0.41	-3.97	ns	-0.09
1.8 m	Peak	7:30	-0.72	-6.54	*	-0.09
1.8 m	Peak	8:00	-1.37	-10.58	***	-0.17
1.8 m	Peak	8:30	-2.42	-15.54	***	-0.32
1.8 m	Peak	9:00	-3.39	-19.03	***	-0.52
1.8 m	Peak	9:30	-3.88	-20.02	***	-0.71
1.8 m	Peak	10:00	-3.58	-17.36	***	-0.74
1.8 m	Peak	10:30	-2.55	-11.96	***	-0.68
1.8 m	Peak	11:00	-1.46	-6.58	***	-0.53
1.8 m	Peak	11:30	0.14	0.64	ns	-0.33
1.8 m	Peak	12:00	0.89	3.85	**	0.01
1.8 m	Peak	12:30	1.57	6.71	***	0.18
1.8 m	Peak	13:00	2.27	9.62	***	0.33
1.8 m	Peak	13:30	2.37	9.89	***	0.46
1.8 m	Peak	14:00	1.73	7.17	***	0.50
1.8 m	Peak	14:30	0.90	3.70	***	0.39
1.8 m	Peak	15:00	0.56	2.32	ns	0.22
1.8 m	Peak	15:30	0.34	1.42	ns	0.13
1.8 m	Peak	16:00	0.26	1.13	ns	0.07
1.8 m	Peak	16:30	0.17	0.75	ns	0.05
1.8 m	Peak	17:00	0.14	0.60	ns	0.03
1.8 m	Peak	17:30	-0.13	-0.60	ns	0.03
1.8 m	Peak	18:00	-0.72	-3.27	**	-0.03
1.8 m	Peak	18:30	-0.99	-4.55	**	-0.18
1.8 m	Peak	19:00	-1.21	-5.66	***	-0.22
1.8 m	Peak	19:30	-1.26	-6.06	***	-0.29
1.8 m	Peak	20:00	-1.08	-5.26	**	-0.29
1.8 m	Peak	20:30	-0.69	-3.55	ns	-0.22
1.8 m	Peak	21:00	-0.52	-2.85	ns	-0.15
1.8 m	Peak	21:30	-0.22	-1.27	ns	-0.12
1.8 m	Peak	22:00	-0.15	-0.92	ns	-0.06
1.8 m	Peak	22:30	-0.20	-1.33	ns	-0.04
1.8 m	Peak	23:00	-0.24	-1.59	ns	-0.05
1.8 m	Peak	23:30	-0.25	-1.73	ns	-0.06

Continued on next page

Table S 3 – *Continued from previous page*

Treatment	Season	Time	Absolute diff.	Percentage diff.	Sig.	Effect size
1.8 m	Shoulder	0:00	-0.53	-8.78	ns	-0.06
1.8 m	Shoulder	0:30	-0.56	-9.79	ns	-0.08
1.8 m	Shoulder	1:00	-0.54	-10.09	ns	-0.08
1.8 m	Shoulder	1:30	-0.55	-10.78	ns	-0.08
1.8 m	Shoulder	2:00	-0.54	-11.45	ns	-0.08
1.8 m	Shoulder	2:30	-0.57	-13.00	ns	-0.08
1.8 m	Shoulder	3:00	-0.55	-13.46	ns	-0.08
1.8 m	Shoulder	3:30	-0.54	-14.27	ns	-0.08
1.8 m	Shoulder	4:00	-0.53	-14.73	ns	-0.08
1.8 m	Shoulder	4:30	-0.52	-14.96	ns	-0.08
1.8 m	Shoulder	5:00	-0.51	-15.81	ns	-0.07
1.8 m	Shoulder	5:30	-0.51	-16.86	ns	-0.07
1.8 m	Shoulder	6:00	-0.50	-17.72	ns	-0.07
1.8 m	Shoulder	6:30	-0.48	-18.90	ns	-0.07
1.8 m	Shoulder	7:00	-0.54	-22.49	ns	-0.07
1.8 m	Shoulder	7:30	-0.62	-24.42	ns	-0.08
1.8 m	Shoulder	8:00	-0.92	-27.32	ns	-0.09
1.8 m	Shoulder	8:30	-1.63	-31.50	***	-0.13
1.8 m	Shoulder	9:00	-2.64	-34.16	***	-0.20
1.8 m	Shoulder	9:30	-3.56	-34.60	***	-0.31
1.8 m	Shoulder	10:00	-3.83	-31.55	***	-0.41
1.8 m	Shoulder	10:30	-3.42	-25.52	***	-0.46
1.8 m	Shoulder	11:00	-2.14	-15.13	***	-0.41
1.8 m	Shoulder	11:30	-0.88	-5.96	ns	-0.26
1.8 m	Shoulder	12:00	0.42	2.74	ns	-0.11
1.8 m	Shoulder	12:30	0.99	6.28	ns	0.05
1.8 m	Shoulder	13:00	1.28	7.87	**	0.12
1.8 m	Shoulder	13:30	1.54	9.22	***	0.16
1.8 m	Shoulder	14:00	1.00	5.92	ns	0.19
1.8 m	Shoulder	14:30	0.67	3.95	ns	0.13
1.8 m	Shoulder	15:00	0.43	2.52	ns	0.08
1.8 m	Shoulder	15:30	0.40	2.37	ns	0.06
1.8 m	Shoulder	16:00	0.20	1.22	ns	0.06
1.8 m	Shoulder	16:30	-0.16	-0.99	ns	0.03
1.8 m	Shoulder	17:00	-0.60	-3.70	ns	-0.02
1.8 m	Shoulder	17:30	-1.01	-6.32	**	-0.09
1.8 m	Shoulder	18:00	-1.42	-9.11	***	-0.14
1.8 m	Shoulder	18:30	-1.45	-9.69	***	-0.20
1.8 m	Shoulder	19:00	-1.33	-9.36	**	-0.19
1.8 m	Shoulder	19:30	-1.10	-8.22	*	-0.18
1.8 m	Shoulder	20:00	-0.73	-6.06	ns	-0.14
1.8 m	Shoulder	20:30	-0.58	-5.53	ns	-0.09
1.8 m	Shoulder	21:00	-0.47	-5.12	ns	-0.08

Continued on next page

Table S 3 – *Continued from previous page*

Treatment	Season	Time	Absolute diff.	Percentage diff.	Sig.	Effect size
1.8 m	Shoulder	21:30	-0.41	-5.03	ns	-0.06
1.8 m	Shoulder	22:00	-0.44	-5.80	ns	-0.06
1.8 m	Shoulder	22:30	-0.49	-6.75	ns	-0.06
1.8 m	Shoulder	23:00	-0.48	-6.98	ns	-0.07
1.8 m	Shoulder	23:30	-0.50	-7.79	ns	-0.07
2.4 m	Peak	0:00	-0.30	-2.15	ns	-0.07
2.4 m	Peak	0:30	-0.38	-2.79	ns	-0.09
2.4 m	Peak	1:00	-0.38	-2.80	ns	-0.10
2.4 m	Peak	1:30	-0.38	-2.90	ns	-0.10
2.4 m	Peak	2:00	-0.44	-3.41	ns	-0.09
2.4 m	Peak	2:30	-0.40	-3.22	ns	-0.10
2.4 m	Peak	3:00	-0.45	-3.73	ns	-0.09
2.4 m	Peak	3:30	-0.49	-4.15	ns	-0.10
2.4 m	Peak	4:00	-0.46	-4.06	ns	-0.11
2.4 m	Peak	4:30	-0.46	-4.14	ns	-0.10
2.4 m	Peak	5:00	-0.46	-4.21	ns	-0.11
2.4 m	Peak	5:30	-0.47	-4.44	ns	-0.10
2.4 m	Peak	6:00	-0.49	-4.69	ns	-0.11
2.4 m	Peak	6:30	-0.49	-4.73	ns	-0.11
2.4 m	Peak	7:00	-0.49	-4.81	ns	-0.11
2.4 m	Peak	7:30	-0.78	-7.10	**	-0.11
2.4 m	Peak	8:00	-1.30	-10.06	***	-0.18
2.4 m	Peak	8:30	-2.24	-14.43	***	-0.30
2.4 m	Peak	9:00	-3.31	-18.60	***	-0.50
2.4 m	Peak	9:30	-3.86	-19.92	***	-0.71
2.4 m	Peak	10:00	-4.15	-20.14	***	-0.75
2.4 m	Peak	10:30	-3.78	-17.70	***	-0.75
2.4 m	Peak	11:00	-2.90	-13.07	***	-0.71
2.4 m	Peak	11:30	-1.69	-7.47	***	-0.59
2.4 m	Peak	12:00	0.15	0.66	ns	-0.39
2.4 m	Peak	12:30	0.99	4.25	**	0.02
2.4 m	Peak	13:00	1.74	7.36	***	0.20
2.4 m	Peak	13:30	1.75	7.29	***	0.37
2.4 m	Peak	14:00	0.90	3.74	***	0.41
2.4 m	Peak	14:30	0.15	0.62	ns	0.23
2.4 m	Peak	15:00	0.00	0.00	ns	0.04
2.4 m	Peak	15:30	-0.19	-0.81	ns	0.00
2.4 m	Peak	16:00	-0.18	-0.78	ns	-0.05
2.4 m	Peak	16:30	-0.24	-1.03	ns	-0.05
2.4 m	Peak	17:00	-0.29	-1.28	ns	-0.06
2.4 m	Peak	17:30	-0.72	-3.21	ns	-0.07
2.4 m	Peak	18:00	-1.28	-5.82	***	-0.15
2.4 m	Peak	18:30	-1.60	-7.37	***	-0.29

Continued on next page

Table S 3 – *Continued from previous page*

Treatment	Season	Time	Absolute diff.	Percentage diff.	Sig.	Effect size
2.4 m	Peak	19:00	-1.59	-7.47	***	-0.35
2.4 m	Peak	19:30	-1.37	-6.60	***	-0.37
2.4 m	Peak	20:00	-1.24	-6.03	***	-0.31
2.4 m	Peak	20:30	-1.06	-5.44	***	-0.25
2.4 m	Peak	21:00	-0.54	-2.96	ns	-0.23
2.4 m	Peak	21:30	-0.39	-2.33	ns	-0.12
2.4 m	Peak	22:00	-0.27	-1.73	ns	-0.11
2.4 m	Peak	22:30	-0.30	-1.95	ns	-0.08
2.4 m	Peak	23:00	-0.33	-2.23	ns	-0.08
2.4 m	Peak	23:30	-0.37	-2.60	ns	-0.09
2.4 m	Shoulder	0:00	-0.60	-9.92	ns	-0.10
2.4 m	Shoulder	0:30	-0.62	-10.74	ns	-0.09
2.4 m	Shoulder	1:00	-0.60	-11.13	ns	-0.09
2.4 m	Shoulder	1:30	-0.60	-11.95	ns	-0.09
2.4 m	Shoulder	2:00	-0.59	-12.67	ns	-0.09
2.4 m	Shoulder	2:30	-0.62	-14.25	ns	-0.08
2.4 m	Shoulder	3:00	-0.61	-15.04	ns	-0.09
2.4 m	Shoulder	3:30	-0.61	-16.00	ns	-0.09
2.4 m	Shoulder	4:00	-0.60	-16.54	ns	-0.09
2.4 m	Shoulder	4:30	-0.58	-16.70	ns	-0.09
2.4 m	Shoulder	5:00	-0.58	-17.91	ns	-0.08
2.4 m	Shoulder	5:30	-0.59	-19.43	ns	-0.08
2.4 m	Shoulder	6:00	-0.56	-20.03	ns	-0.08
2.4 m	Shoulder	6:30	-0.55	-21.42	ns	-0.08
2.4 m	Shoulder	7:00	-0.61	-25.36	ns	-0.08
2.4 m	Shoulder	7:30	-0.67	-26.51	ns	-0.09
2.4 m	Shoulder	8:00	-0.92	-27.50	ns	-0.10
2.4 m	Shoulder	8:30	-1.59	-30.85	***	-0.13
2.4 m	Shoulder	9:00	-2.56	-33.07	***	-0.19
2.4 m	Shoulder	9:30	-3.41	-33.14	***	-0.30
2.4 m	Shoulder	10:00	-3.92	-32.24	***	-0.40
2.4 m	Shoulder	10:30	-4.01	-29.86	***	-0.47
2.4 m	Shoulder	11:00	-3.30	-23.36	***	-0.48
2.4 m	Shoulder	11:30	-2.24	-15.15	***	-0.40
2.4 m	Shoulder	12:00	-0.68	-4.46	ns	-0.27
2.4 m	Shoulder	12:30	0.59	3.73	ns	-0.08
2.4 m	Shoulder	13:00	0.97	5.94	ns	0.07
2.4 m	Shoulder	13:30	1.04	6.26	ns	0.12
2.4 m	Shoulder	14:00	0.39	2.33	ns	0.13
2.4 m	Shoulder	14:30	0.10	0.60	ns	0.05
2.4 m	Shoulder	15:00	-0.04	-0.26	ns	0.01
2.4 m	Shoulder	15:30	0.01	0.04	ns	-0.01
2.4 m	Shoulder	16:00	-0.11	-0.63	ns	0.00

Continued on next page

Table S 3 – *Continued from previous page*

Treatment	Season	Time	Absolute diff.	Percentage diff.	Sig.	Effect size
2.4 m	Shoulder	16:30	-0.60	-3.62	ns	-0.01
2.4 m	Shoulder	17:00	-1.12	-6.86	**	-0.08
2.4 m	Shoulder	17:30	-1.60	-10.04	***	-0.15
2.4 m	Shoulder	18:00	-1.92	-12.34	***	-0.22
2.4 m	Shoulder	18:30	-1.80	-12.03	***	-0.26
2.4 m	Shoulder	19:00	-1.56	-10.93	***	-0.24
2.4 m	Shoulder	19:30	-1.29	-9.63	**	-0.21
2.4 m	Shoulder	20:00	-0.85	-7.13	ns	-0.16
2.4 m	Shoulder	20:30	-0.72	-6.81	ns	-0.11
2.4 m	Shoulder	21:00	-0.54	-5.87	ns	-0.10
2.4 m	Shoulder	21:30	-0.49	-5.94	ns	-0.07
2.4 m	Shoulder	22:00	-0.51	-6.68	ns	-0.07
2.4 m	Shoulder	22:30	-0.54	-7.51	ns	-0.07
2.4 m	Shoulder	23:00	-0.54	-7.88	ns	-0.08
2.4 m	Shoulder	23:30	-0.57	-8.87	ns	-0.07